Journal Pre-proof

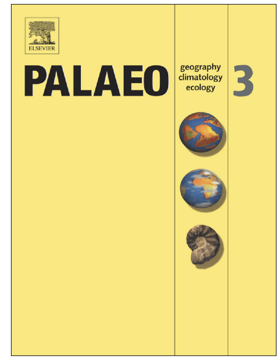

Landslide clusters in the Tovel Valley (Brenta Dolomites, N Italy) triggered by far field earthquakes?

Sandro Rossato, Silvana Martin, Susan Ivy-Ochs, Alfio Viganò, Giovanni Monegato, Giacomo Prosser, Christof Vockenhuber, Manuel Rigo

PII: S0031-0182(26)00643-7

DOI: https://doi.org/10.1016/j.palaeo.2026.114180

Reference: PALAEO 114180

To appear in: *Palaeogeography, Palaeoclimatology, Palaeoecology*

Received date: 5 June 2026

Revised date: 27 August 2026

Accepted date: 27 August 2026

Please cite this article as: S. Rossato, S. Martin, S. Ivy-Ochs, et al., Landslide clusters in the Tovel Valley (Brenta Dolomites, N Italy) triggered by far field earthquakes?, *Palaeogeography, Palaeoclimatology, Palaeoecology* (2026), https://doi.org/10.1016/j.palaeo.2026.114180

Landslide clusters in the Tovel Valley (Brenta Dolomites, N Italy) triggered by far field earthquakes?

Sandro Rossato[1], Silvana Martin[2], Susan Ivy-Ochs[3,4], Alfio Viganò[5], Giovanni Monegato[1], Giacomo Prosser[6], Christof Vockenhuber[4], Manuel Rigo[2,1]

[1] Institute of Geosciences, National Research Council of Italy, Corso Stati Uniti 4, 35127 Padova, Italy

[2] Department of Geosciences, University of Padova, Via Gradenigo 6, 35131 Padova, Italy

[3] Department of Earth Sciences and Planetary Sciences, ETH Zürich, Sonneggstrasse 5, 8092 Zürich, Switzerland

[4] Laboratory of Ion Beam Physics, ETH Hönggerberg, Otto-Stern-Weg 5, 8093 Zürich, Switzerland

[5] Servizio Geologico, Provincia autonoma di Trento, Via Zambra 42, 38121 Trento, Italy

[6] Dipartimento di Scienze, Università Della Basilicata, Via Dell'Ateneo Lucano, 10 - 85100, Potenza, Italy

Corresponding author: Sandro Rossato - sandro.rossato@cnr.it

Abstract

Large blocky landslide deposits are widespread in Alpine valleys of northern Italy, yet their timing, emplacement history, and geomorphic significance remain debated. In the Tovel Valley (Brenta Dolomites, Italy), extensive blocky accumulations have been variously attributed to deglaciation or to younger slope-failure events, with important implications for valley evolution and hazard assessment. This study aims to determine the timing, sequence, and emplacement relationships of the main deposits, evaluate their role in valley damming and the evolution of Lake Tovel, and assess long-term drivers and short-term triggers within a regional Alpine context.

We combine detailed geomorphological mapping with analysis of LiDAR-derived topography and orthophotos, supported by cosmogenic ^{36}Cl exposure dating of boulders from six deposits. Exposure ages indicate Holocene emplacement and suggest two broad periods of landslide activity. The older phase is represented by a principal Mid-Holocene age population centred at 5.21 ± 0.16 ka, together with overlapping chronological constraints from other deposits, whereas younger exposure ages fall between ~1.0 and ~0.6 ka. Integration of exposure ages with superposition relationships, morphology, lithology, and inferred source areas allows reconstruction of a relative landslide sequence involving repeated independent failures from both valley flanks.

The distribution and volumes of the deposits suggest that several events were capable of partially or fully damming the valley, consistent with a multi-phase history including lake formation, drainage reorganization, and renewed damming at Lake Tovel. The landslides reflect persistent long-term predisposing factors, including carbonate lithology affected by karst dissolution, inherited structural anisotropies, and glacial and paraglacial modification, while temporal clustering suggests episodic short-term triggering during periods of heightened susceptibility. Seismic shaking is considered the most plausible regional-scale trigger for the younger cluster, whereas trigger attribution for older events remains uncertain. Overall, the Tovel Valley provides an illustrative case study of Holocene large landslides in an Alpine carbonate setting, highlighting the value of integrating geomorphic analysis with cosmogenic dating to resolve landslide sequences and valley evolution.

Keywords

Landslides; Holocene; Cl-36 cosmogenic dating; European Alps; Carbonate rocks; Brenta Dolomites; Lake Tovel

1. Introduction

European Alpine valleys host numerous large rockslide deposits produced by catastrophic or rapid slope-failure events (also termed “Sturzstroms” in the German literature and “rock avalanches” in the English one), which have long attracted the attention of engineers and geoscientists and the concern of local authorities because of their potential impact on inhabitants and infrastructure. Large rock failures involving millions of cubic meters are relatively rare, yet many have been studied in detail owing to their landscape-scale effects and hazard significance (e.g., Heim, 1932; Montandon, 1933; Abele, 1974; 1994; Prager et al., 2008; Stead and Wolter, 2015). Less voluminous landslides, on the order of less than ~1 million cubic meters, can also threaten lives and infrastructure and therefore merit attention (e.g., Aldighieri et al., 2016). An in-depth understanding of past events, including their emplacement style, dynamics, timing, and potential for recurrence, is essential for assessing territorial vulnerability (Samia et al., 2017). In this paper, we distinguish drivers (long-term preconditioning factors) from triggers (short-term initiating factors). Common triggers include seismic shaking (e.g., the 2008 Wenchuan earthquake, China; Yin et al., 2009), changes in pore pressure due to exceptional rainfall (e.g., Loew et al., 2017), and human intervention (e.g., the Vajont rock avalanche, Italy; Wolter et al., 2016).

The Trento Province includes the Brenta Dolomites, one of the most renowned and touristic mountain areas of the Italian Alps (UNESCO World Heritage; https://www.dolomitiunesco.info/). This region hosts several large landslide deposits (Fig. 1), including Gorte (estimated volume ~90 Mm^3; Perna, 1991; Ruggia et al., 2021), Lavini di Marco (~200 Mm^3; Martin et al., 2014), Marocca Principale and Kas (~1000 Mm^3 and ~300 Mm^3, respectively; Ivy-Ochs et al., 2017a), and Molveno (~600 Mm^3; von Wartburg et al., 2020). Smaller deposits related to historical detachments are also present in the area (Fig. 1). In this contribution, we use landslide as a generic term for slope-failure events, rock avalanche for rapid, long-runout rock failures that produce extensive blocky accumulations, deposit for the resulting geomorphic body, and event when referring to the episode(s) as a whole.

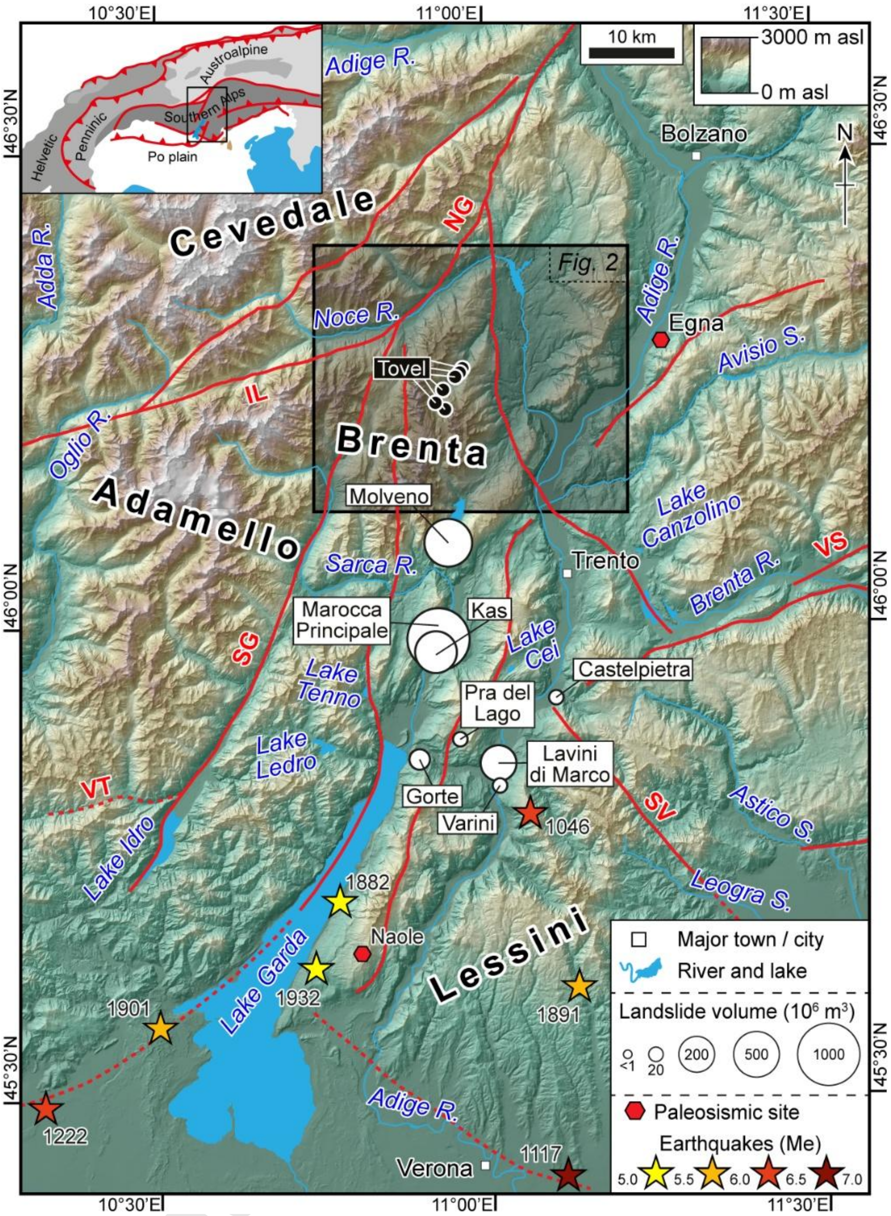

Figure 1: context map of the study area. Major landslides are marked, along with the main faults traversing the bedrock (IL, Insubric Line; NG, North Giudicarie; SG, South Giudicarie; SV, Schio-Vicenza; VS, Valsugana), selected sites with published evidence of paleoseismic activity, Holocene surface deformation, or archaeoseismic evidence (Galadini et al., 2001; Sauro and Zampieri, 2001; Livio et al., 2009; Berlusconi et al., 2013), and the epicenters of the historical earthquakes cited in the text (colour-coded stars labelled by event year; Guidoboni et al., 2018, 2019). The location of Fig. 2 is indicated by the black shaded box. The background DEM is the freely available TINItaly dataset (Tarquini et al., 2007, 2023; https://tinitaly.pi.ingv.it/).

Historically, many Alpine blocky deposits were interpreted as glacially transported debris (e.g., Lepsius, 1878; Abele, 1997) and attributed to deglaciation following the Last Glacial Maximum (LGM, 26.5-19 ka cal BP; Clark et al., 2009), with ice decay in the region estimated after 18,500 cal BP (Ravazzi et al., 2014;

Ivy-Ochs, 2015; Rettig et al., 2025). In the eastern Italian Alps, these large blocky accumulations in the past were referred to as *Marocche* (e.g., Trevisan, 1939; Perna and Sauro, 1979). Over recent decades, isotopic dating has shown that several such deposits in the Alps are Holocene in age (e.g., Ostermann et al., 2017; Ivy-Ochs et al., 2009; Martin et al., 2014; Ivy-Ochs et al., 2017b; Viganò et al., 2021; Ruggia et al., 2021). This pattern suggests the possibility that comparable drivers may have operated under Holocene climate conditions broadly similar to the present and that similar events may occur in the future, making the understanding of their triggering factors pivotal for land management.

The northernmost valley of the Brenta Dolomites, the Tovel Valley, hosts extensive blocky deposits spanning ~4.5 km^2 with a total volume of 200-280 Mm^3 (Oetheimer, 1989; 1990, and references therein). These deposits have been recognized and discussed since the late 19^{th} century (e.g., de Mortillet, 1861; Taramelli, 1881; Trevisan, 1939; Sacco, 1940). They have been variously interpreted as *Marocche* formed during the decay of the Würm glaciation (e.g., Trevisan, 1939; Sacco, 1940; Oetheimer, 1989; 1990) or as accumulations linked to subsequent landscape evolution (Stoppani, 1878; Damian, 1892; Penk and Bruckner, 1909; Schwinner, 1912; Trener, 1924; Wiebols, 1938; Venzo, 1960; Fuganti, 1969; Chardon, 1975; Perna and Sauro, 1979). To date, there is no published numerical dating for these deposits, and their chronology remains debated (Dal Piaz et al., 2007). Accordingly, competing hypotheses include emplacement during LGM deglaciation, Holocene emplacement, or a multi-event sequence with possible post-depositional deformation and reworking. Because such alternatives have different implications for the geomorphic evolution of the valley, chronology is central to the present study.

The Brenta Dolomites are prone to exceptional climatic events (Benito et al., 2015) and lie within a seismically active sector of the Southern Alps connected to the Giudicarie and Schio-Vicenza fault systems (Slejko et al., 1989; Viganò et al., 2015), factors that can act as triggers for slope failures. Historical earthquakes and paleoseismic evidence from the Garda-Baldo-Lessini sector and the adjacent Po Plain indicate that strong seismic shaking has repeatedly affected a wide region extending to the study area (Galadini et al., 2001; Sauro and Zampieri, 2001; Livio et al., 2009; Berlusconi et al., 2013; Scardia et al., 2015). Against this regional backdrop, our objectives are to determine the origin of the Tovel Valley blocky deposits, clarify their emplacement dynamics and number of events, and evaluate their triggers. To this aim, we present new geomorphic analyses, cosmogenic nuclide exposure dating, and lithological analyses of the boulders belonging to these deposits. We also assess geomorphic evidence for valley damming and its implications for the evolution of Lake Tovel, consider the temporal relations among events (including the possibility of clustering), and examine the plausibility of earthquake triggering in a regional context (including far-field effects). Finally, we discuss the occurrence of these landslides relative to coeval events in the Trentino area and to cases from comparable settings, thereby situating the Tovel Valley within the broader Alpine pattern.

2. Setting

2.1 Geography and geology

The Brenta Dolomites are located between the Rendena and Meledrio Valleys to the west and the Non Valley to the east, in the central Southern Alps. The massif (~550 km^2) is incised by N-S to NNE-SSW valleys (Fig. 2). One of these is the Tovel Valley, which descends from Cima Falkner (2999 m a.s.l.) to Tuenno (630 m a.s.l.) at its junction with the Non Valley, a major tributary of the Adige Valley (Fig. 2). To the south, the head of the Tovel Valley separates it from the Seghe Valley, which terminates at Lake Molveno, dammed by a large rock avalanche deposit dated to 4.8 ± 0.5 ka (von Wartburg et al., 2020; Fig. 2). The Tovel Valley is ~17 km long and comprises an upper reach, a wider central sector hosting Lake Tovel and the main blocky deposits, and a narrow lower reach extending toward Tuenno.

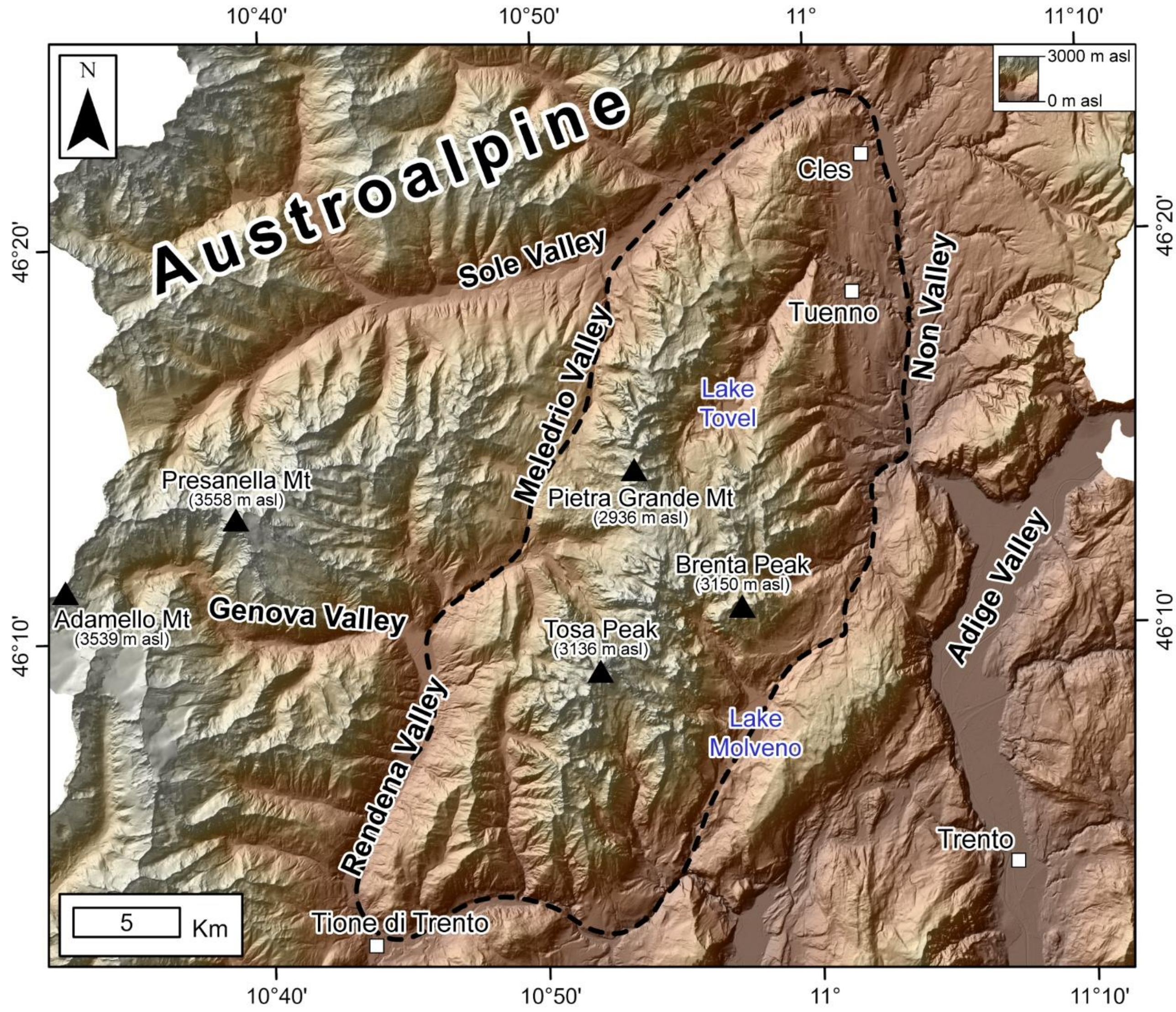

Figure 2: elevation map of the study area, highlighting major cities, peaks, and valleys. The boundary of the Brenta Massif is outlined by a dotted black line. Major peaks are showed. The background DEM is derived from the freely available TINItaly dataset (Tarquini et al., 2007, 2023; https://tinitaly.pi.ingv.it/).

The valley is carved into a thick Upper Triassic-Lower Jurassic carbonate succession belonging to the western sector of the Trento Platform, close to its transition toward the Lombardian Basin, and affected by inherited Jurassic extensional structures (Castellarin, 1972; Doglioni and Bosellini, 1987; Picotti et al., 1998; Prosser, 2000; Castellarin et al., 2006). Inherited Jurassic normal faults, including the Palete, Flavona, Pra de l'Asen and Val Strangola structures, segment the carbonate succession and locally juxtapose different lithological units (Fig. 3). Upper Triassic dolomitic carbonates and Lower Jurassic limestones dominate both valley flanks, although important lithological contrasts exist between them. The eastern slope includes Jurassic and Cretaceous pelagic formations (e.g. TOF, EPE, ARV, MAI and SAA), whereas the western slope is largely dominated by DPR, ZUU and the Calcari Grigi Group (Figs. 3 and 4). These contrasts are important for reconstructing source areas and lithological provenance of the landslide deposits discussed below. A complete lithostratigraphic framework and the abbreviations of geological units used throughout the manuscript are shown in Fig. 3.

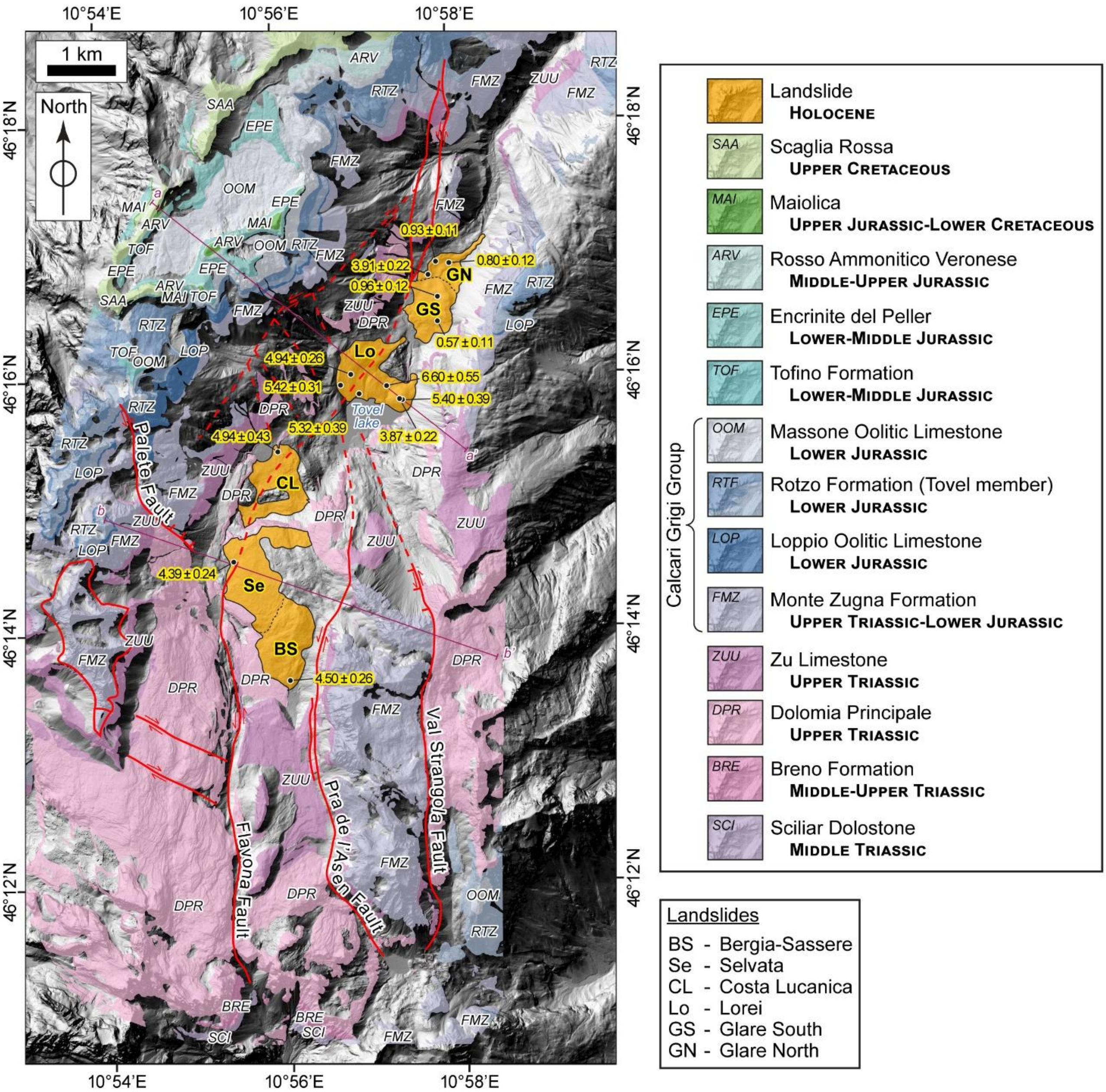

Figure 3: geological map of the study area, showing outcropping , major faults, and landslide bodies. Cosmogenic sampling locations are indicated by black dots, and corresponding ^{36}Cl exposure ages are highlighted in yellow. The traces of the two geological profiles reported in Figure 5 are shown in purple.

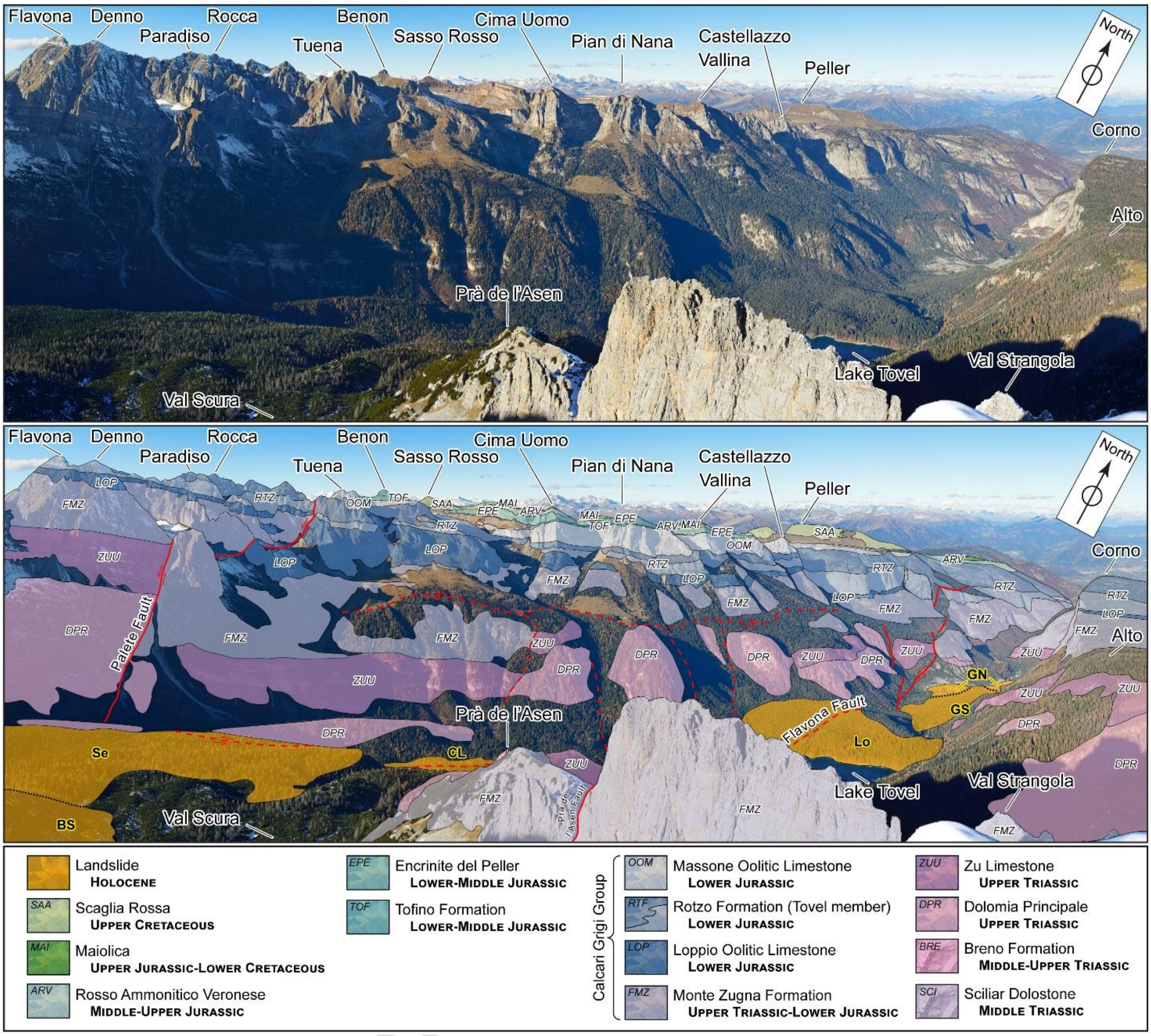

Figure 4: panorama of the western flank of the Tovel Valley. The upper frame shows the original photograph, while the lower frame superimposes geological formations onto the image. Photo courtesy of M. Visintainer.

The overall stratigraphic pile dips gently (10-20°) to the WNW (Fig. 5). The combination of thick carbonate successions, inherited normal-fault architecture, Alpine tectonic reactivation, and widespread karstification generated litho-structural anisotropies and weakened rock masses on both valley flanks. These factors constitute major predisposing conditions for slope failure and help explain the occurrence of large blocky landslide deposits throughout the valley.

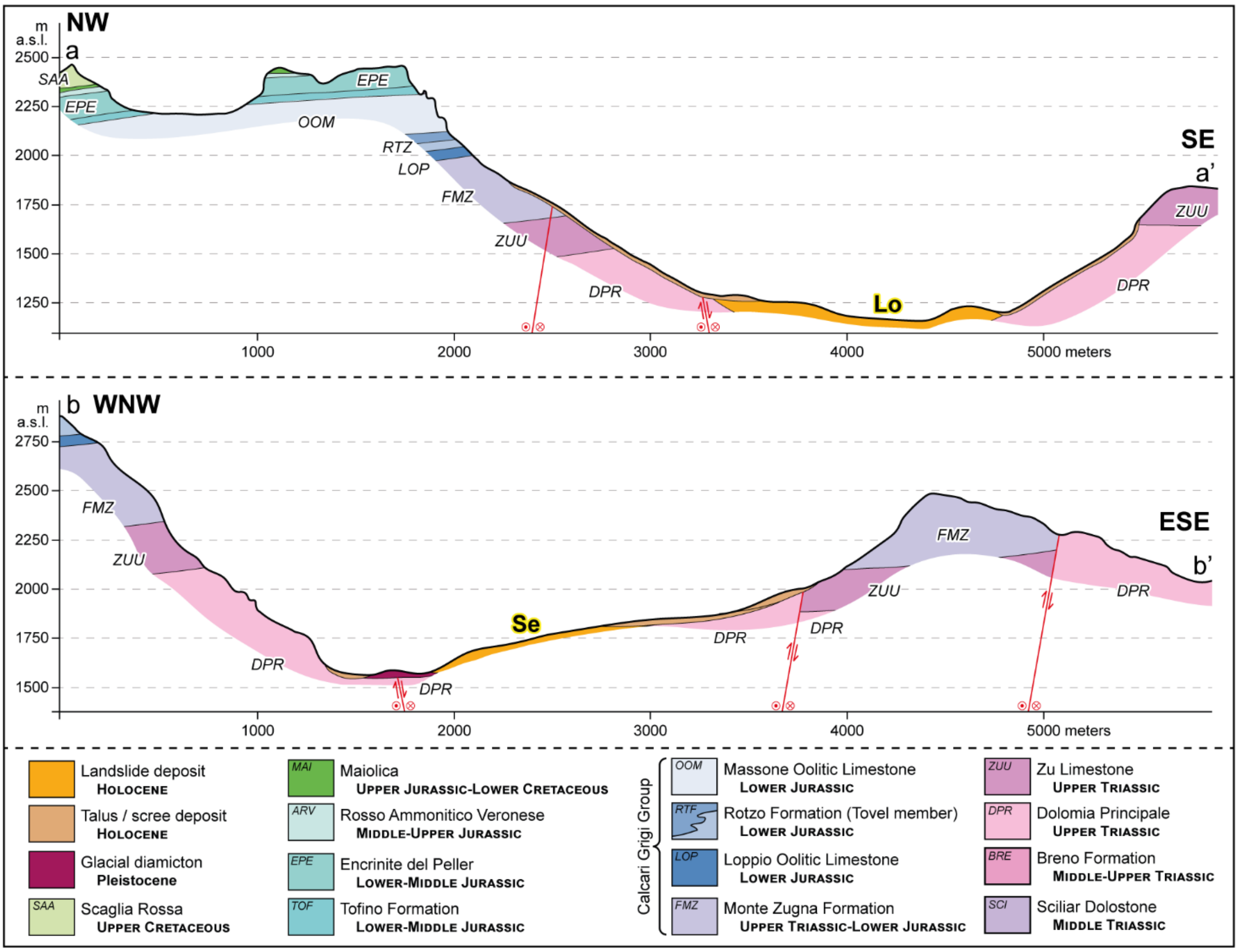

Figure 5: geological profiles across the Tovel Valley in the area north of Lake Tovel (a-a') and across the southern plateaux (b-b'). The traces are shown in Fig. 3.

Alpine tectonics reactivated Jurassic faults, developing pervasive cleavages and foliations (Prosser, 1998; Castellarin et al., 2006), and promoted localized erosion and karst formation since pre-Quaternary times (Borsato, 2007; Audra et al., 2006; Sauro et al., 2021). Neotectonic activity of the Giudicarie and Schio-Vicenza fault systems (Castellarin et al., 2006; Viganò et al., 2015), superimposed on long-term Quaternary deformation of the southern Alpine margin (Scardia et al., 2015; Aghib et al., 2024), has been associated with seismicity whose effects are recognized even far from the epicentral areas (Guidoboni et al., 2018, 2019), mostly along major faults (Viganò et al., 2015). Regional tectonic studies indicate that active deformation is accommodated by fault systems in the Garda-Veronese sector and the adjacent Po Plain, where several structures have been proposed as potentially seismogenic sources for strong historical earthquakes (Berlusconi et al., 2013; Scardia et al., 2015). Over the last ~70 years, several earthquakes reached Moment Magnitude (Mw) 4.5 (Rovida et al., 2020, 2022): "Valli Giudicarie" (19 Feb 1960, Mw 4.8), "Val Lagarina" (22 Jun 1968, Mw 4.7), "Garda Settentrionale" (13 Dec 1976, Mw 4.9), "Garda Occidentale" (24 May 1987, Mw 4.6), "Prealpi Vicentine" (13 Sep 1989, Mw 4.85), "Val Venosta" (17 Jul 2001, Mw 4.8; Caporali et al., 2005), "Garda Occidentale" (24 Nov 2004, Mw 5). Archaeological evidence and chronicles document additional significant earthquakes with Equivalent Magnitudes (Me) ≥ 5 in a broader area (Fig. 1; Guidoboni et al., 2018, 2019): "Media valle dell'Adige" (9 Nov 1046; Me 6.0), "Veronese" (3 Jan 1117; Me 6.8), "Basso bresciano" (25 Dec 1222; Me 6.0), "Monte Baldo" (18 Sep 1882; Me 5.0), "Valle d'Illasi" (7 Jun 1891; Me 5.9), "Salò" (30 Oct 1901; Me 5.7), "Monte Baldo" (19 Feb 1932; Me 5.1). The "Media valle dell'Adige" and "Veronese" events fall within the uncertainty of stalagmite failures at Cogola di Giazzera cave, near the Lavini di Marco landslide (Fig. 1; 1060 ± 70 AD; Frisia et al., 2005). At the Egna archaeological site (Fig. 1), two earthquakes are inferred: an older one post-dating a soil displacement radiocarbon-dated to 2830-2237 cal BC, and a younger (Mw 6.3-6.5) event around the mid-3rd century AD, responsible for site abandonment (Galadini and Galli, 1999) and recorded also at Lake Monticolo Piccolo (Niederstätter et al., 2025).

Additional evidence of late Quaternary and Holocene tectonic activity is available elsewhere in the region. Paleoseismological trenching at the Naole and Orsara fault scarps in the Mt Baldo-Lessini sector documented repeated Late Quaternary surface deformation, although chronological constraints remain broad and some structures may have a gravitational component (Galadini et al., 2001; Sauro and Zampieri, 2001). In the Brescia piedmont area, active fault-related folding, surface faulting and liquefaction features associated with the Capriano del Colle fault system indicate persistent tectonic activity and strong local earthquakes during the late Quaternary (Livio et al., 2009). Regional syntheses further identify several capable fault systems in the Lake Garda area and discuss their possible role in generating major historical earthquakes, including the AD 1117 and AD 1222 events (Berlusconi et al., 2013; Scardia et al., 2015).

2.2 Geomorphology and Late Pleistocene/Holocene evolution

The Tovel Valley hosts a diverse suite of glacial and periglacial landforms, alluvial and lacustrine deposits, karst features, and chaotic gravitational debris masses, including landslide deposits (Dal Piaz et al., 2007 and references therein; Fig. 6). Most glacial landforms and deposits are attributed to the LGM, during which the valley-glacier network attained thicknesses of several hundred meters in the Tovel Valley (Dal Piaz et al., 2007). Today, in response to recent temperature rise, no permanent glaciers persist.

The Brenta Dolomites represent the largest underground hydrogeological structure in the Trento Province (Borsato, 2007). Controlled by regional tectonics, the massif hosts nearly 500 karst cavities, including multi-kilometre shafts, especially in its central and southern sectors. Widespread karst landforms and cave systems testify to a long-lasting karst evolution that predates the Quaternary (Borsato, 2007; Sauro et al., 2021).

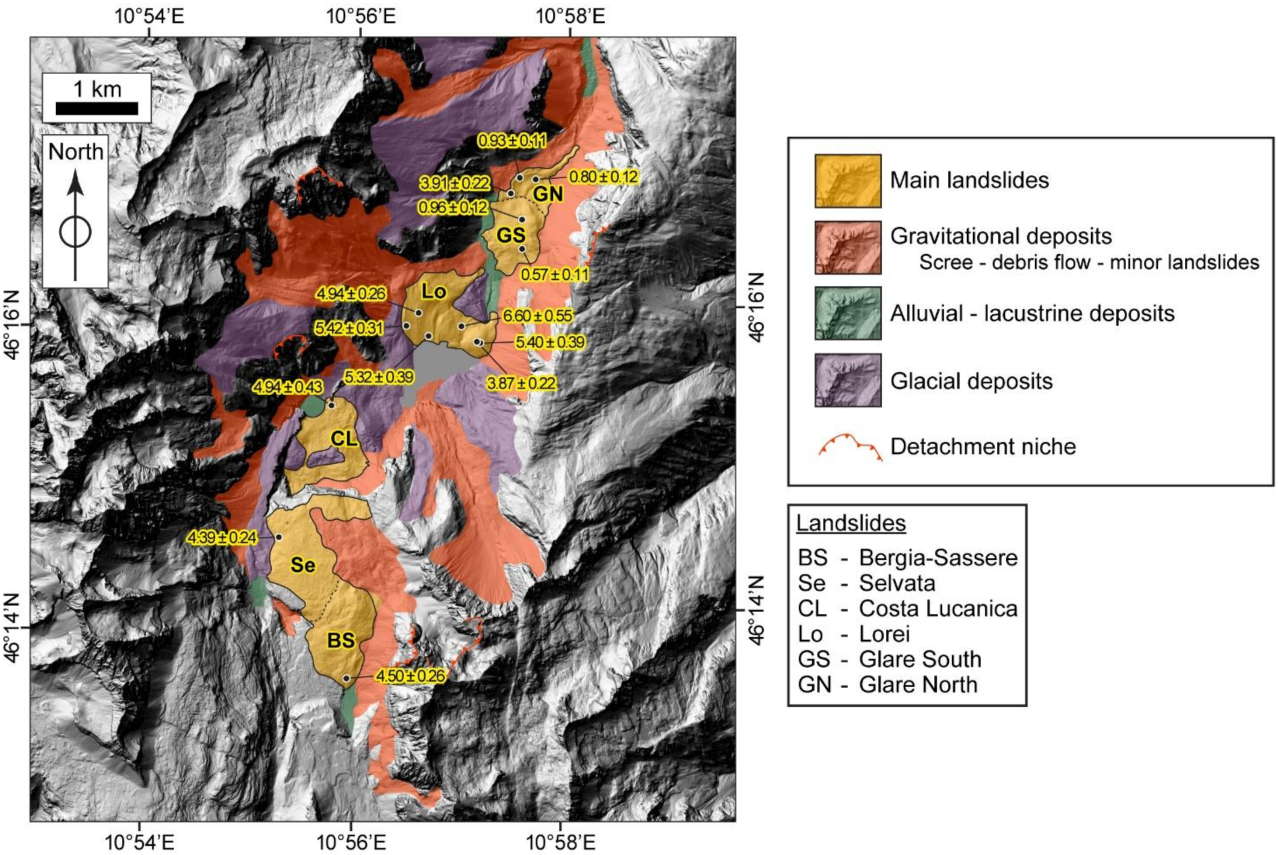

Figure 6: map of the central stretch of the Tovel Valley. The main Quaternary deposits are reported, together with the investigated landslide deposits. Cosmogenic sampling locations are indicated by black dots, and corresponding ^{36}Cl exposure ages are shown for each sampled boulder.

The upper valley is up to nearly 2 km wide and has an asymmetrical cross-section. To the west, the Grostè plateau (~3 km^2) is bounded by a ~350-m-high, nearly vertical slope that forms the left flank above the valley bottom (the Flavona plateau). The latter is a glacially moulded surface covered by alpine meadows (1800-2200 m a.s.l.). The headwall is irregular, with isolated peaks and saddles up to ~3000 m a.s.l. The eastern slope consists of a ~3-km-long cliff from Monte Fibbion (2673 m a.s.l.) to Cima di Val Scura (2670 m a.s.l.), connected to the valley floor by extensive talus. Where bedrock is exposed, roches moutonnées and glacial cirques dominate. On flat surfaces, colluvial, swamp, and lacustrine deposits occur, like the Lac Sec area (~5 ha), which borders the Bergia area to the south (Fig. 7).

Figure 7: photographs of landslide deposits: (a) Lac Sec, looking north; beyond it, the Bergia-Sassere deposit is visible on the right. (b) Boundary between the Selvata deposit (left) and the Bergia-Sassere deposit (right). (c) Selvata deposit. (d) Costa Lucanica deposit. (e) Karst features on a boulder from the Lorei deposit (TOV4). (f) Glare area: the barren Glare North deposit in the foreground and the vegetated Glare South deposit in the background.

The Grostè and Campo Flavona plateaux exhibit a glacio-karst landscape with endorheic depressions, sinkholes, and surface karst morphologies (e.g., corridors and crevasses; Nicod, 1976; Borsato, 2001), together with glacially furrowed fields (Ferretti and Borsato, 2006a). Karst development is most advanced in DPR and ZUU, guided by fracture networks and enhanced by intense meteoric infiltration (Borsato et al., 2000), with additional dissolution along fractures and faults. Karst springs at plateaux margins sustain the upper Tresenga Stream (Fig. 7; Borsato and Ferretti, 2004).

The central valley (~3 km wide) displays a classic U-shaped profile (Figs. 5, 8) with two prominent longitudinal steps. The upper step (~200-m vertical drop) separates Costa Lucanica and Selvata (1627-1454 m a.s.l.). The lower step (1178-1035 m a.s.l.) lies between Lorei and Glare, near the lake (Fig. 3). The western slope drops ~1400 m, incised by deep gullies feeding talus cones and scree; the eastern slope, ~1000 m high, is largely mantled by scree and is interrupted only by Val Strangola, which terminates at the SE shore of Lake Tovel, forming a fan delta (Fig. 6). The majority of the blocky deposits in the Tovel Valley occur in this reach, infilling the valley bottom together with remnants of LGM/Lateglacial deposits (Dal Piaz et al., 2007).

The western side of the valley hosts an extensive karst network that promotes infiltration of rainfall and snowmelt and contributes to complex groundwater circulation within the catchment (Borsato et al., 2000). This system feeds both Lake Tovel and the main surface drainage network and is responsible for multiple stream sink and resurgence zones along the valley (Borsato and Ferretti, 2004).

Lake Tovel covers 0.38 km^2, has a maximum depth of 39 m, and holds 7.4 Mm^3 of water (Kulbe et al., 2005). Lake Tovel was formerly known for periodic red algal blooms, which ceased in 1964 following changes in agricultural practices that reduced nutrient input (Baldi, 1941; Fuganti and Morteani, 1999), the lake also contains a submerged forest, similar to those in Lakes Molveno, Tenno, Cei, and Canzolino (Fig. 1). Uprooted *Abies alba* trees, first noted by Freshfield (1875), yielded radiocarbon ages of 1283-1421 AD (Barbina et al., 1984); later dendrochronology indicated a sudden lake-level rise between winter 1597 and summer 1598 (Kulbe et al., 2005; Camagna et al., 2021). Subsurface stratigraphy (Kulbe et al., 2005) shows the drowned forest rooted in coarse-grained deposits interpreted as a mass-flow, overlying a >4-m-thick silty-clayey sequence of lacustrine-to-palustrine facies down to 1132 m a.s.l. The origin of Lake Tovel remains debated: either Lateglacial, related to a postglacial depression and changes in debris permeability (e.g., Oetheimer, 1989), or much younger (1597-1598 AD), linked to minor rock-slope failures that dammed the outflow (e.g., Ferretti and Borsato, 2006b). The lower reach is a narrow, V-shaped bedrock gorge and does not show any remnants of landslide accumulation (Dal Piaz et al., 2007).

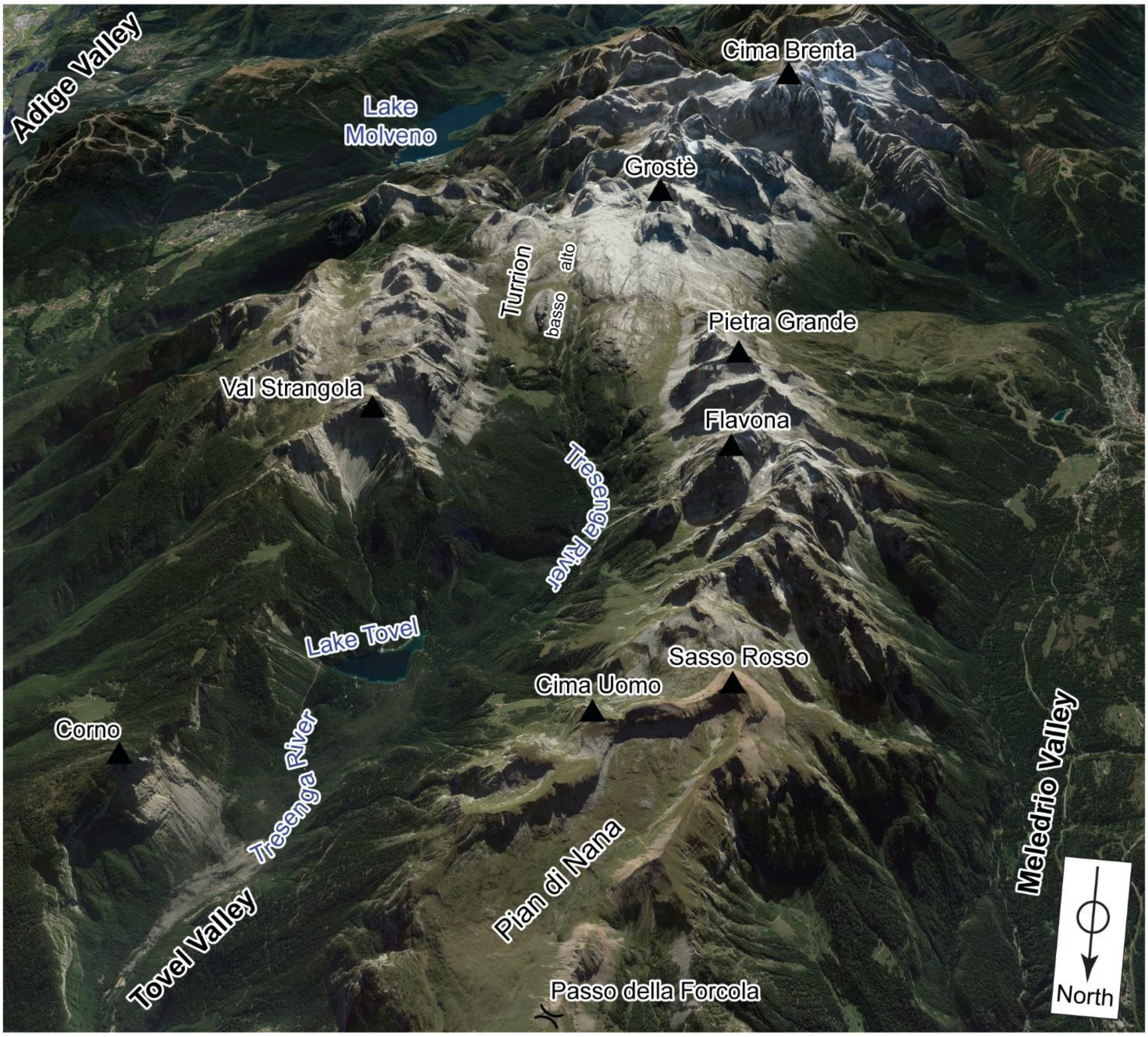

Figure 8: inclined view of the study area, with satellite imagery draped over the SRTM DEM (Google Earth).

Glacial overdeepening and step-like longitudinal geometry focus sediment storage on the central reach, where blocky landslide deposits from both flanks accumulated and interacted with karst-modulated hydrology. The narrow lower reach provides an efficient outlet, whereas the steps and valley narrows constitute potential damming points that align with the observed lake-level history. These inherited glacial and karst boundary conditions, together with Holocene processes, frame later discussion of multi-event landslides, deposit sequencing/clustering, and valley damming.

3. Materials and methods

3.1 Field survey and remote sensing

The rocky deposits of the Tovel Valley were investigated by geomorphological field mapping, outcrop description, and interpretation of aerial and satellite images (Google Earth and Bing databases). Orthophotos and the 1-m LiDAR Digital Terrain Model (DTM) freely distributed by the Autonomous Province of Trento were used throughout (https://siat.provincia.tn.it/stem/, last access: 15 March 2026). The topographic profiles shown in the paper, as well as the area estimates, are based on these datasets.

Lithologies of the deposits were inferred from field observations and thin-section analyses. In the field, deposits were classified on the basis of macroscopic fossils and sedimentary structures. Sixteen boulders were sampled from the deposits for cosmogenic ^{36}Cl exposure dating to constrain the timing of deposit emplacement. The number of samples and their association with mapped deposits are reported in Table 1. Deposits are treated methodologically as single-event emplacement surfaces for exposure-age purposes unless stratigraphic or geomorphic evidence indicates otherwise; potential inheritance and reworking are recognized limitations and are evaluated in the Discussion.

A detailed micropaleontological analysis was carried out on the samples selected for geochronological dating (see Supplementary Data). Major and trace element concentrations determined by ICP-MS (Table 2) complement these observations by verifying lithological assignments used in the exposure-age calculations and providing elemental inputs required for production from major elements and for low-energy neutron capture pathways considered in the ^{36}Cl production model.

Sample name	Lithology	Latitude North [°]	Longitude East [°]	Elevation [m a.s.l.]	Sample thickness [cm]	Topographic shielding	^{36}Cl [10^5 atoms/gram]	Apparent Exposure Age [ka]
TOV1	FMZ	46.2273	10.9353	1872	2	0.934	3.94 ± 0.19	4.50 ± 0.26
TOV2	ARV	46.2426	10.9240	1601	2	0.937	3.28 ± 0.14	4.39 ± 0.24
TOV3	FMZ	46.2564	10.9328	1330	2	0.968	2.22 ± 0.17	4.94 ± 0.43
TOV4	ARV	46.2649	10.9539	1174	2	0.969	2.56 ± 0.18	6.60 ± 0.55
TOV5	FMZ	46.2795	10.9625	999	2	0.922	1.75 ± 0.08	3.91 ± 0.21
TOV6	ARV	46.2633	10.9563	1236	2	0.969	2.19 ± 0.11	3.87 ± 0.22
TOV7	DPR	46.2643	10.9486	1194	2	0.975	2.13 ± 0.12	5.32 ± 0.39
TOV8	FMZ	46.2670	10.9473	1259	2	0.882	2.64 ± 0.11	4.94 ± 0.26
TOV9	FMZ	46.2659	10.9449	1252	2	0.961	3.13 ± 0.15	5.42 ± 0.31
TOV10	ARV/TOF	46.2640	10.9570	1235	3	0.926	2.07 ± 0.12	5.40 ± 0.39
TOV12	FMZ	46.2740	10.9640	1110	3	0.952	0.30 ± 0.06	0.57 ± 0.11
TOV14	FMZ	46.2770	10.9640	1060	3	0.951	0.48 ± 0.06	0.96 ± 0.12
TOV15	FMZ	46.2810	10.9660	970	2	0.947	0.37 ± 0.06	0.80 ± 0.12
TOV16	FMZ	46.2810	10.9630	1010	4	0.953	0.44 ± 0.05	0.93 ± 0.11

Table 1: samples collected from boulders in the Tovel valley deposits. The site information, the ^{36}Cl exposure ages, and the lithology of the boulder based on thin sections are given. Shielding includes surrounding topography and dip of sampled surface.

Sample name	SiO2 [%]	Al2O3 [%]	Fe2O3 [%]	MnO [%]	MgO [%]	CaO [%]	Na2O [%]	K2O [%]	TiO2 [%]	P2O5 [%]	Sm [ppm]	Gd [ppm]	Th [ppm]	U [ppm]	Cl [ppm]
TOV1	0.8	0.36	0.14	0	0.88	53.2	0.04	0.1	0.02	< 0.01	0.1	0.1	0.2	0.4	19.38 ± 0.06
TOV2	1	0.38	0.06	0	1.17	54.1	0.15	0.1	0.01	< 0.01	< 0.1	< 0.1	< 0.1	1.3	26.73 ± 0.06
TOV3	0.6	0.28	0.11	0.01	18.6	32.4	0.08	0.1	0.01	< 0.01	0.2	0.1	0.1	2.5	48.81 ± 0.11
TOV4	0.4	0.19	0.09	0	21.1	30.5	0.04	0	0.01	< 0.01	< 0.1	< 0.1	< 0.1	4.4	53.09 ± 0.15
TOV5	1.2	0.5	0.08	0	0.48	54.7	0.18	0.1	0.01	< 0.01	< 0.1	< 0.1	< 0.1	0.3	10.01 ± 0.02
TOV6	0.4	0.16	0.13	0.01	2.83	52.9	0.04	0	0	< 0.01	0.1	< 0.1	< 0.1	4.2	20.47 ± 0.05
TOV7	0.3	0.12	0.08	0.01	20.7	31.2	0.03	0	0	0.01	< 0.1	0.1	< 0.1	< 0.1	51.42 ± 0.14
TOV8	1	0.44	0.06	0	0.54	55.1	0.16	0.1	0	< 0.01	< 0.1	< 0.1	< 0.1	0.3	14.04 ± 0.06
TOV9	0.5	0.26	0.08	0	0.59	55	0.05	0.1	0.01	< 0.01	0.2	0.2	0.2	0.8	14.61 ± 0.12
TOV10	1.3	0.52	0.63	0.01	19.1	31.5	0.04	0.2	0.02	< 0.01	0.3	0.2	0.3	0.9	44.66 ± 0.32
TOV12	0.4	0.19	0.12	0.01	0.67	54.9	0.03	0	0.01	0.02	0.1	< 0.1	0.1	0.2	20.48 ± 0.52
TOV14	2.1	1.11	0.31	0.01	0.57	52.7	0.04	0.3	0.05	0.04	0.7	0.7	0.7	0.3	23.69 ± 0.14
TOV15	1	0.49	0.11	0.01	0.68	54.3	0.04	0.1	0.03	< 0.01	0.3	0.2	0.4	0.4	23.53 ± 0.30
TOV16	0.5	0.17	0.07	0	0.6	54.9	0.03	0	0.01	0.02	< 0.1	< 0.1	0.1	0.2	16.78 ± 0.10

Table 2: elemental composition of leached samples. Cl values are from AMS measurements.

3.2 Cosmogenic ^{36}Cl exposure dating

Sample preparation followed isotope-dilution procedures as described by Ivy-Ochs et al. (2004). Total Cl and ^{36}Cl were determined in the same target at the ETH AMS facility of the Laboratory for Ion Beam Physics (LIP) with the 6 MV tandem accelerator. Sample ^{36}Cl /Cl ratios were normalized to the ETH internal standard K382/4N with a value of ^{36}Cl /Cl = 17.36 × 10^{-12}, calibrated against the primary ^{36}Cl standard KNSTD5000 (Christl et al., 2013; Vockenhuber et al., 2019). Full process chemistry blanks (3.4 × 10^{-15}) were subtracted from measured sample ratios.

Surface exposure ages were calculated with the LIP ETH in-house MATLAB code based on parameters presented in detail in Alfimov and Ivy-Ochs (2009) and references therein. A production rate of 48.8 ± 3.4 ^{36}Cl atoms (g Ca)$^{-1}$ yr^{-1} was used, which encompasses a muon contribution at the rock surface of 9.6%; and a value of 760 ± 150 neutrons (g air)$^{-1}$ yr^{-1}. Production from all major elements and through low-energy neutron capture, in light of the trace elements, was fully considered. Production rates were scaled to the latitude, longitude, and altitude of the sites based on Stone (2000). No additional corrections for topographic shielding, snow cover, or vegetation apply.

No correction was made for karst weathering of the boulder surfaces (cf. Styllas et al., 2018). Field observations indicate that the extent of karst dissolution on boulder surfaces varies significantly from boulder to boulder but can be estimated as less than 2 cm. A sensitivity test implementing a rate of 5 mm/ka would change the ages by less than 2%, which is within the range that does not alter the interpretations presented. Stated errors of the exposure ages (Table 1) include both analytical uncertainties and those of the production rates (Alfimov and Ivy-Ochs, 2009).

Ages are interpreted as emplacement-related exposure where boulders rest on landslide deposits; inheritance is a known limitation in carbonate settings and is addressed in the Discussion. ICP-MS geochemistry supports lithological verification and provides the elemental compositions required for pathway-specific ^{36}Cl production terms in the calculations. The approach maintains consistency with the mapping framework used in Section 3.1 and the scaling scheme of Stone (2000), without introducing further corrections or assumptions beyond those stated above.

For deposits dated by multiple boulders, the internal consistency of exposure ages was evaluated using inverse-variance weighted means, chi-square statistics, and reduced chi-square values (χ^2red). In addition, leave-one-out sensitivity analyses were performed to assess the influence of individual samples on the overall age distribution. These analyses were used to evaluate whether individual exposure ages could be treated as a statistically coherent population and to identify samples contributing disproportionately to age scatter. Statistical results were considered together with geomorphological and lithological evidence.

For deposits represented by a single dated boulder, the obtained exposure age was interpreted as a weak chronological constraint consistent with deposit emplacement. Such ages provide information on the timing of surface exposure but do not allow statistical evaluation of age variability within the deposit and should therefore not be regarded as robust depositional ages.

4. Results: Tovel Valley blocky deposits, inferred source areas, and exposure ages

The blocky deposits mapped in the Tovel Valley cover an area of approximately 5 km^2 and extend for nearly 9 km along the valley, between the Pozzoi waterfall to the lower part of the central valley reach (Fig. 3), between elevations of ~1950 m and ~900 m a.s.l. (Fig. 3). Deposit thickness is not directly observable because basal contacts are not exposed. Based on their mapped distribution, morphology, texture, and lithology, the deposits were subdivided into six areas, from south to north: Bergia-Sassere, Selvata, Costa Lucanica, Lorei, Glare South, and Glare North (Fig. 3). The surrounding slopes of the central reach contain several large detachment niches, as well as smaller niches on both valley sides at multiple elevations.

4.1 Bergia-Sassere

The Bergia-Sassere blocky deposit is the southernmost and highest deposit in the valley and is located on the eastern side of the valley between ~1940 and ~1800 m a.s.l. (Figs. 3, 6). It covers an area of ~0.83 km^2 and consists predominantly of FMZ boulders. The deposit is composed of angular boulders ranging from meter to several meters in size, arranged in an openwork fabric with sparse pebbles and sandy matrix. It forms two adjacent vegetated (mainly shrubs and dwarf pines) mounds that rise above the surrounding surface: the Bergia mound to the south (1895 m a.s.l.; ~15 m-high; ~0.31 km^2) and the Sassere mound to the north (1940 m a.s.l.; ~80 m-high; ~0.52 km^2). Secondary semi-circular scarps are present along the western margin of the deposit.

The eastern margin of the Bergia-Sassere deposit is locally overlain by scree sourced from the valley slope, whereas the southernmost edge borders the swampy lacustrine setting of Lac Sec (Fig. 7a). The approximate volume of the deposit is reported as ~145 Mm^3 (Oetheimer, 1989), largely associated with the Sassere mound. The mapped distribution, restricted to the eastern valley side, the absence of comparable debris accumulation on the western side, and the mound-like morphology are consistent with limited lateral spreading. The inferred source area is a ~900-m-long, near-vertical cliff extending from ~2050 and ~2500 m a.s.l., composed of tectonised thin levels of ZUU at the base and FMZ above ~2160 m a.s.l. (Figs. 5, 6). Sampling for cosmogenic dating was performed on boulder TOV1, collected from the top of the Bergia mound. The boulder is composed of FMZ and displays karst corrosion features, including karren up to ~2 cm deep (Fig. 9a). The measured exposure age is 4.50 ± 0.26 ka. As only one boulder was dated, this age should be treated carefully, as a chronological constraint consistent with deposit emplacement rather than a robust depositional age.

Figure 9: selected photos of sampled boulders. A: Bergia-Sassere (TOV1); B: Selvata (TOV2); C: Costa Lucanica (TOV3); D: Lorei (TOV4), E: Lorei (TOV7); F: Dos del Lago (TOV6), G: Glare North (TOV5).

4.2 Selvata

The Selvata blocky deposit lies immediately west of the Bergia-Sassere deposit and covers ~1.2 km^2 on a plateau bounded to the north and west by vertical cliffs (Fig. 3, 4, 5, 6). The deposit is dominated by FMZ boulders, with subordinate DPR and ZUU blocks. Its surface is broadly planar, with an average slope of ~25% and a predominant westward dip (Fig. 10). The deposit includes a blocky lower part extending down to the Tresenga Stream and an upper part composed of smaller angular boulders and blocks. A pebble-sandy matrix is abundant throughout the deposit.

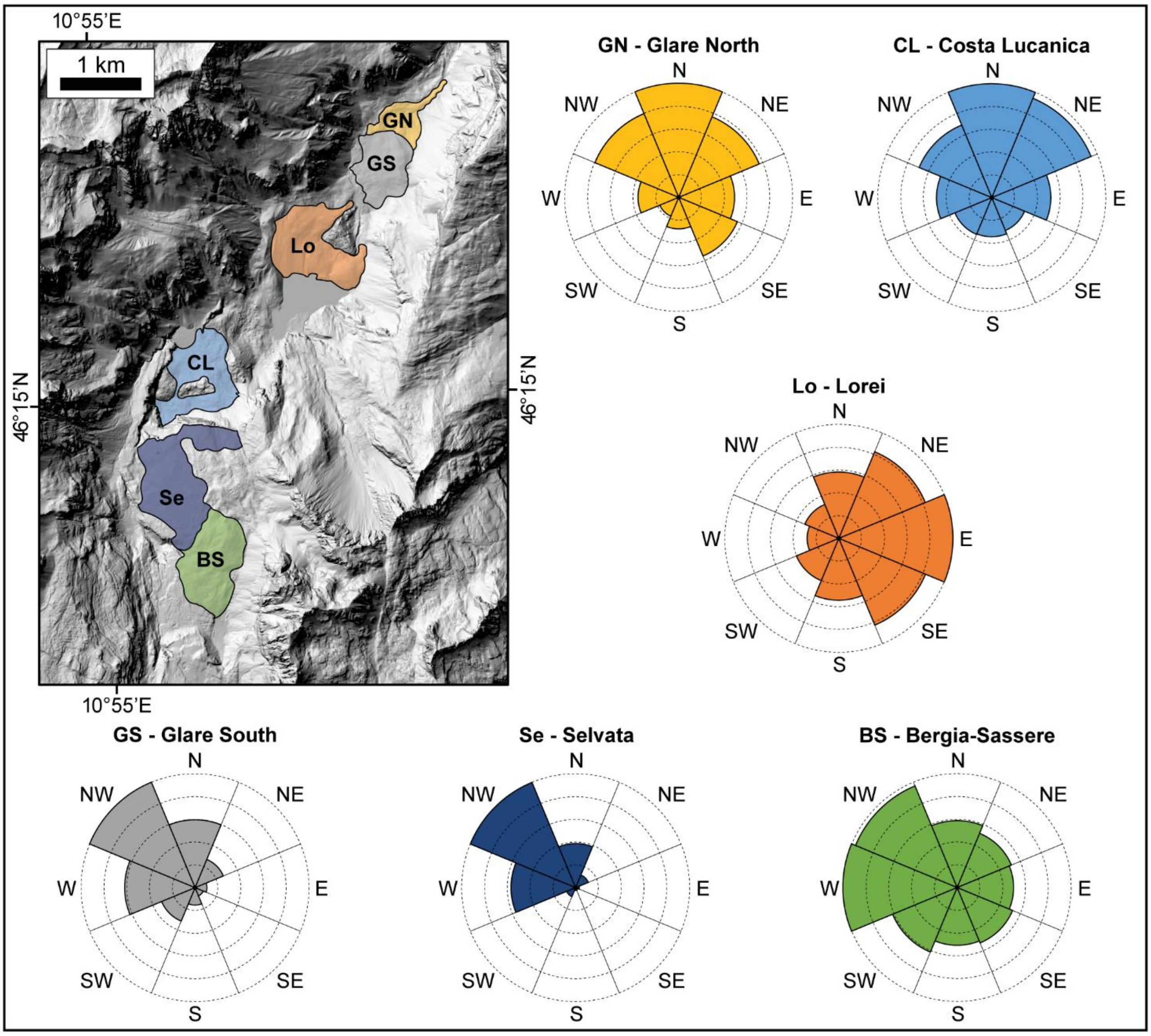

Figure 10: Radargrams showing the dipping directions of deposits (45° bins), identifying three main groups: North-dipping (Glare North, Costa Lucanica), East-dipping (Lorei), West and Northwest-dipping (Glare South, Selvata, and Bergia-Sassere).

The southeastern boundary of the Selvata deposit is defined by partial overlap by the Bergia-Sassere deposit (Fig. 7b). The surface is densely vegetated, with tall trees, and boulders are widely covered by mosses and lichens. The eastern sector is buried by debris-flow deposits fed by Val Scura (Figs. 3, 4, 5, 6). Based on bedrock trends in adjacent areas, a mean thickness of 10 m is hypothesized, corresponding to an approximate volume of ~12 Mm^3, reported as a minimum because of burial in the eastern sector.

The gentle and persistent westward slope of the deposit surface is consistent with an inferred source area in Val Scura. The detachment niche is reported as encompassing the headwall of Val Scura between 2250 and 2600 m a.s.l. (Fig. 6). An H/L ratio of ~0.33 was calculated; together with the estimated deposit volume, this supports classification of the event as a rock avalanche (Aaron and McDougall, 2019).

Cosmogenic dating was performed on boulder TOV2, sampled from the lower part of the deposit at 1601 m a.s.l. (Fig. 9b). The boulder is composed of ARV and yielded an exposure age of 4.39 ± 0.24 ka. The nearest documented ARV outcrop is located farther north along the western valley side below Cima Uomo at ~2400 m a.s.l. (Fig. 3, 4). The presence of an ARV boulder within the Selvata deposit is therefore not readily explained by the currently inferred source-area reconstruction. The sampled boulder may represent material incorporated into the moving mass during transport, implying a potentially complex exposure history, although alternative explanations cannot be excluded. Accordingly, the 4.39 ± 0.24 ka exposure age is compatible with emplacement of the Selvata deposit but, because the sampled boulder has uncertain provenance, it is not regarded as a robust depositional age.

4.3 Costa Lucanica

In the Costa Lucanica area, a blocky deposit occurs between ~1450 and ~1300 m a.s.l., beneath the upper valley step at 1627-1454 m a.s.l. that separates this sector from Selvata. The deposit covers approximately 0.5 km^2 and rests on DPR bedrock (Fig. 3). It contains FMZ angular boulders several meters in size and meter-sized angular DPR blocks. Clasts are highly fragmented and embedded in abundant pebbles and sandy matrix. A distinctive textural feature is a layer of large boulders resting on glacial sediments (Dal Piaz et al., 2007).

The surface of the deposit supports forest vegetation, with tall trees and shrubs, and boulders are covered by centimetre-thick mosses and lichens (Fig. 7d). The overall dip of the deposit is toward the north-northeast. Debris accumulation is preferentially developed on the western sides of bedrock and glacial ridges in the valley bottom, resulting in an asymmetric distribution across the valley floor and pointing to a source area on the left valley flank (Fig. 3, 6). A rough volume estimate is based on a mean thickness of 10 m, which, combined with the mapped area, corresponds to a volume of ~5 Mm^3.

An inferred detachment niche occurs at ~1600-1840 m a.s.l. (Fig. 6). Owing to its proximity to the Flavona fault (Fig. 3), bedrock in the inferred source area may have been affected by subsidiary faulting and associated fracturing. The debris was funnelled towards the valley bottom and spread across a broad area, indicating high mobility. Boulder TOV3 was sampled at 1331 m a.s.l. and identified by thin-section analysis as FMZ. The reported MgO content of 18.6% (Table 2) indicates some degree of dolomitization, consistent with macroscopic field observations. The boulder yielded an exposure age of 4.94 ± 0.43 ka. As only one boulder was dated, this age should be treated carefully, as a chronological constraint consistent with deposit emplacement rather than a robust depositional age.

4.4 Lorei

The Lorei blocky deposit spans approximately 0.85 km^2 between ~1100 and ~1300 m a.s.l. and includes deposits bordering Lake Tovel to the north and northwest, locally extending downslope over portions of the downstream step (1035-1177 m a.s.l.; Fig. 3, 4, 6). Northeast of the lake, the deposit forms the mound-like Dos del Lago, which rises to ~50 m above lake level. The deposit is composed mainly of Jurassic limestones ranging from FMZ to ARV, consistent with lithologies exposed in the left valley wall between Cima Uomo and Cima Vallina (Fig. 3, 4, 5).

The deposit surface displays arcuate ridges and incisions with concavity facing west and an overall dip toward the east-northeast (Figs. 5, 10). In the central sector, W-E-aligned scarps up to ~2 m high and ~300 m long are present, while the western sector contains semi-circular depressions up to ~5 m deep and ~90 m long, bounded by well-defined counterscarps. Post-depositional deformation features in the central and western sectors are interpreted as possibly related to seasonal ground-ice formation. The deposit consists of angular boulders ranging from meter to several meters in size, with pebbles arranged in an openwork structure and filled by a medium-to-scarce sandy matrix. Vegetation near the lake is characterized by patchy stands of tall trees and shrubs.

Deposit thickness is variable. If the fine-grained lacustrine sediments beneath the modern lake accumulated within a basin dammed by the Lorei deposit, and considering valley-side geometry and erosional scarps along the deposit boundary, a mean deposit thickness of ~100 m can be estimated, corresponding to a total volume of ~85 Mm^3. The modern lake partially covers the deposit. To the west, the deposit is locally overlain by alluvial sediments delivered by streams descending the valley flank, which also incise the northernmost sector. Additional incisions separate the deposit from adjacent glacial deposits to the west and from a triangular patch of blocky deposits and bedrock in the central valley sector (Fig. 6). The easternmost incision is occupied by the Tresenga Stream, which flows from the lake.

Based on boulder lithologies and deposit dip, the detachment niche is placed on the western valley side between 2400 and 2000 m a.s.l. A ~900 m long niche is hypothesized east of Cima Uomo (Fig. 6), where ARV may have been exposed before slope failure. An H/L ratio of ~0.43 was calculated; together with the estimated volume, this supports classification of the deposit as a rock-avalanche deposit (Aaron and McDougall, 2019).

Six boulders were sampled for cosmogenic dating (Fig. 9d-f): ARV (TOV4, TOV6), ARV/TOF (TOV10), DPR (TOV7), and FMZ (TOV8, TOV9). Exposure ages of 6.60 ± 0.55 ka, 3.87 ± 0.22 ka, 5.40 ± 0.39 ka, 5.32 ± 0.39 ka, 4.94 ± 0.26 ka, and 5.42 ± 0.31 ka were obtained. Statistical evaluation of the age distribution (Supplementary Data – Appendix B) indicates that the six ages do not form a single internally consistent population (χ^2red = 7.38). The observed scatter is dominated by TOV6 and, secondarily, by TOV4. A sensitivity analysis shows that the four central ages (TOV7, TOV8, TOV9, and TOV10) form a statistically coherent group with a weighted mean age of 5.21 ± 0.16 ka (χ^2red = 0.62). Accordingly, the complete six-boulder dataset is not used to define a single exposure age for the Lorei deposit, whereas the weighted mean of the four statistically coherent central ages provides the principal chronological estimate evaluated in the Discussion.

4.5 Glare (South and North)

The Glare deposits comprise all blocky deposits downstream of the Lorei deposit, between ~900 and ~1130 m a.s.l., and occupy the right side of the valley. The lower part of the deposits is incised by the Tresenga Stream. Two bodies are distinguished, Glare South and Glare North, based on vegetation abundance and the presence of a scarp marking their contact (Figs. 3, 4, 6, 7f).

Glare South extends from ~1130 m a.s.l. downslope to the Tresenga Stream, approximately 130 m lower, and covers an area of ~0.4 km^2. The deposit is composed of meter-sized angular boulders of FMZ and ZUU, with pebbles and sandy matrix. Its upper part displays a hilly morphology, whereas the lower part is more planar, with a gradient of ~20% dipping predominantly to the northwest (Fig. 10). Vegetation consists of sparse tall trees and abundant shrubs. A mean thickness of 25 m is hypothesized based on valley-slope geometry outside the deposit, yielding a volume of ~10 Mm^3. The deposit dip and boulder lithologies point to a detachment niche at the top of the eastern valley slope between 1800 and 1500 m a.s.l. (Fig. 6). Cosmogenic dating was performed on two meter-sized FMZ boulders, TOV12 and TOV14, which yielded exposure ages of 0.57 ± 0.11 ka and 0.96 ± 0.12 ka, respectively. Both ages indicate Late Holocene surface exposure, although their difference relative to the associated uncertainties does not support treatment as a single statistically coherent age population. The two ages are therefore considered individually rather than combined into a depositional age.

Glare North occupies the valley floor between ~1050 and ~900 m a.s.l., covers approximately 0.25 km^2, and overlies the northern edge of Glare South. It consists of meter-sized angular FMZ boulders arranged in an openwork structure with scarce sandy matrix and almost no vegetation. The deposit includes a long ridge, slightly concave to the east, rising up to ~30 m and extending for ~0.6 km, as well as a second, smaller ridge located farther east (Fig. 6). With a hypothesized mean thickness of 20 m, the reported volume is ~5 Mm^3. The northwestward dip and boulder lithologies of the Glare deposits are consistent with source areas on the eastern valley side (Figs. 5, 10). The base of the rock walls is mantled by talus cones continuously supplied by small failures and rockfalls. The inferred Glare North source area lies along the same rock wall as that inferred for Glare South (Fig. 6). A very large FMZ boulder (TOV5) sampled from Glare North yielded an exposure age of 3.91 ± 0.21 ka and displays multiple fracture sets intersecting bedding (Fig. 9g). Two additional metric FMZ boulders (TOV15, TOV16) yielded exposure ages of 0.80 ± 0.12 ka and 0.93 ± 0.11 ka, respectively. The anomalously old age of TOV5 is interpreted as most likely reflecting inherited preexposure, whereas TOV15 and TOV16 form a statistically coherent population considered more representative of deposit emplacement, and indicate Late-Holocene exposure ages comparable to those obtained for Glare South.

5. Discussion

5.1 Landslide sequence and implications for the evolution of Lake Tovel

The six landslides analysed in this work produced blocky deposits that, by their position in the valley bottom, would have been capable of partially or completely damming the Tovel Valley at different times. Each deposit is morphologically distinct, and the cosmogenic ^{36}Cl boulder exposure ages span from 6.60 ± 0.55 to 0.57 ± 0.11 ka, covering nearly six millennia (Table 1). Because these are boulder surface-exposure ages, their correspondence with deposit emplacement depends on the exposure history of each sampled surface. They are therefore interpreted as emplacement-related chronological evidence rather than as exact event ages, with possible inheritance, erosion, shielding, reworking, and re-exposure considered where relevant. For deposits dated by multiple boulders, exposure ages are discussed individually and evaluated using inverse-variance weighted means and chi-square statistics to assess internal consistency. Where age scatter exceeds that expected from analytical uncertainties, results are interpreted cautiously and in conjunction with geomorphological evidence. Collectively, the new ^{36}Cl ages and geomorphological relationships support predominantly Holocene emplacement of the mapped landslide sequence, challenging earlier interpretations that assigned these deposits to the Lateglacial (Dal Piaz et al., 2007 and references therein).

When considering individual deposits, Lorei provides the oldest well-constrained principal exposure-age population among the investigated deposits. The six Lorei exposure ages do not form a single statistically coherent population. However, four central ages define a coherent principal population with a weighted mean of 5.21 ± 0.16 ka, supporting Middle Holocene emplacement of the deposit. Single-boulder exposure ages from Costa Lucanica (4.94 ± 0.43 ka) and Bergia-Sassere (4.50 ± 0.26 ka) provide Middle Holocene chronological constraints broadly overlapping, within uncertainty, with the principal Lorei age population. The Selvata age (4.39 ± 0.24 ka) is also compatible with this interval, although its interpretation requires additional caution because of the uncertain provenance of TOV2. In terms of relative sequence from geomorphic relationships, Bergia-Sassere partially overlies Selvata, demonstrating that it postdates Selvata irrespective of the overlapping uncertainties of their single-boulder exposure ages. Downstream, Glare South and Glare North yield several Late Holocene exposure ages between 0.57 and 0.96 ka. The two younger Glare North samples form a coherent population around 0.9 ka, whereas the Glare South ages show greater dispersion and are considered individually. Geomorphic superposition demonstrates that Glare North postdates Glare South, although the exposure ages do not resolve the time interval between the two events. Overall, the data indicate a Holocene sequence in which multiple deposits are chronologically close and therefore cannot always be strictly ordered by exposure ages alone; in these cases, superposition relationships and geomorphological evidence provide complementary constraints.

One sample deserves explicit caution: TOV2, collected from the Selvata deposit, consists of ARV lithologies that are not exposed within the currently inferred source area of the deposit (Fig. 3, 5). Consequently, the representativeness of this boulder as a direct chronometer of the Selvata event cannot be demonstrated unequivocally. Nevertheless, the obtained exposure age of 4.39 ± 0.24 ka is consistent with the Middle Holocene ages identified elsewhere in the valley and with the geomorphological evidence indicating that Selvata predates the overlying Bergia-Sassere deposit. A possible explanation is that TOV2 represents material incorporated into the moving mass during transport. In this context, it is noteworthy that glacier ice can substantially enhance rock-avalanche mobility (Aaron and McDougall, 2019). An earlier transport episode during LGM deglaciation could therefore have displaced ARV material from the Sasso Rosso-Cima Uomo sector into positions later involved in the Selvata failure. Under such a scenario, the sampled surface may have been refreshed during the rock-avalanche event and subsequently exposed. However, the available evidence does not allow discrimination among this and other possible explanations. Accordingly, TOV2 is best regarded as a chronological constraint compatible with a Middle Holocene emplacement of the Selvata deposit rather than as a definitive depositional age.

The evolution of Lake Tovel provides an important test for the valley-damming implications of the dated deposits. The depression hosting Lake Tovel has been interpreted as a Lateglacial kettle hole by Oetheimer (1989) and subsequent studies. Although a glacially inherited depression cannot be excluded, the Holocene chronology of the Lorei deposit indicates that the present basin geometry and damming history cannot be explained solely by a Lateglacial origin. Seismic and stratigraphic investigations of the lake bottom document up to 4 m of laminated lacustrine sediments transitioning to palustrine deposits (Kulbe et al., 2005). Although the age of this sedimentary sequence is unknown and has been interpreted as Lateglacial in previous work, its elevation is consistent with the possible base level of a Lorei-related dam. One plausible interpretation is that emplacement of Lorei created or modified a dammed basin in which lacustrine sedimentation occurred, followed by shallowing and palustrine development that supported a surrounding forest. A change from permanent lake to marsh could reflect partial breaching or re-organization of the outlet through or around the Lorei deposit, allowing drainage and the development of a terrestrial forest habitat in the depression.

The drowning of this forest during the winter of 1597-1598 records a subsequent, abrupt rise in lake level (Oetheimer, 1990; Camagna et al., 2021). Proposed explanations include changes in debris permeability and/or in the feeding karst system (Oetheimer, 1989; Bertagnoli et al., 2006; Ferretti and Borsato, 2006b), or damming of the lake outlet by a rockfall (Kulbe et al., 2005; Ferretti and Borsato, 2006b). Camagna et al. (2021) show that the drowned-forest distribution is more consistent with the absence of a lake immediately prior to drowning, implying a larger water-level rise than previously assumed. Within that framework, a possible scenario is that the submerged ridge hosting much of the drowned forest could itself be a landslide body that temporarily dammed the outlet and produced the modern lake; the abundance of collapsed trees is consistent with strong disturbance (Fig. 11; Camagna et al., 2021). This scenario remains a working hypothesis at present, but it highlights that the sedimentary and geomorphic record may reflect recurrent damming episodes in the same sector of the valley, consistent with the stratigraphic evidence for at least two lacustrine phases. These may represent repeated partial damming and re-establishment of the outlet system, rather than a single long-lived lake.

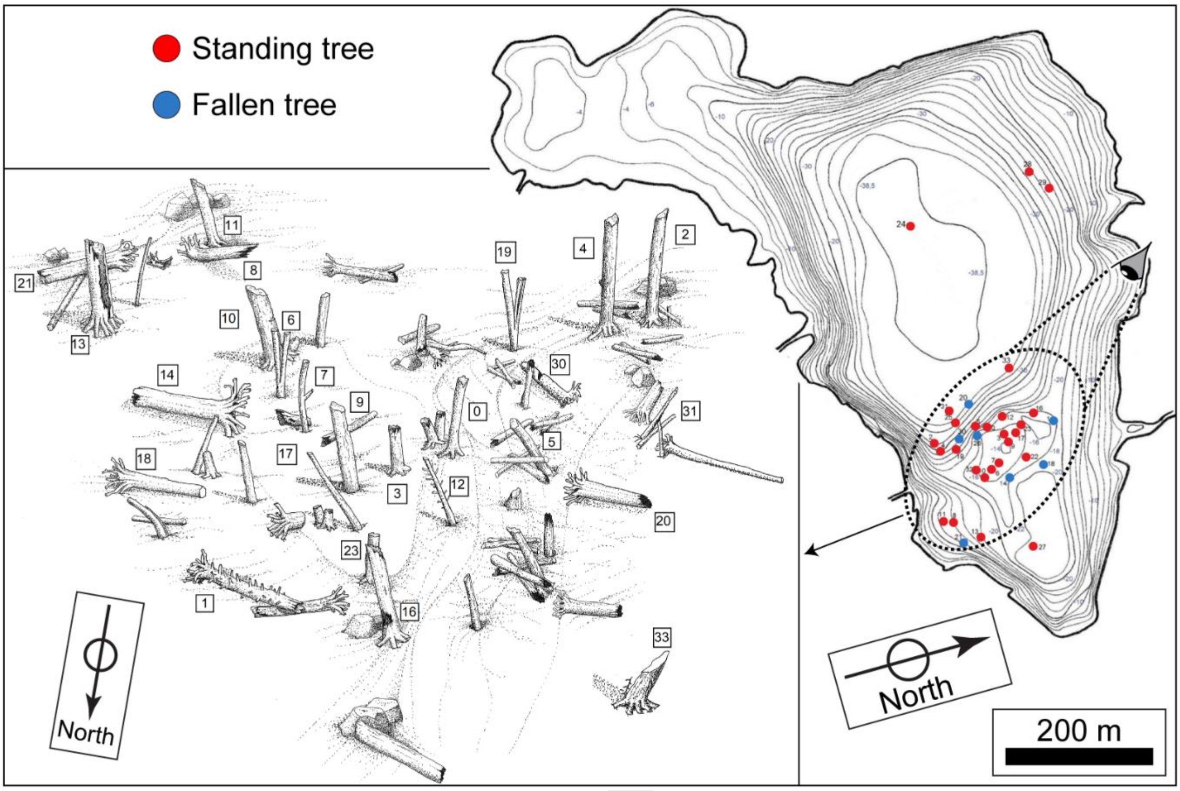

Figure 11: bathymetry map of the Lake Tovel with marked the trees that have been found (red dots: standing; blue: fallen). In the insert is reported an artistic hand-drawing the shows the arrangements of most of the trees (images courtesy of T. Camagna).

5.2 Chronological comparisons with landslides in the Trentino area

Placed in a regional context, the Tovel ages fall within time windows that are comparable to other dated large landslides in Trentino. Dating techniques, materials, and uncertainties listed below differ among studies, so caution is preferred. Eight major events (mostly to the south) display a temporal pattern that broadly resembles that observed at Tovel, with several events occurring during a Middle Holocene interval and others during the Late Holocene. The older group, Dosso Gardene (Martin et al., 2014), Gorte (Ruggia et al., 2021), Marocca Principale (Ivy-Ochs et al., 2017a), and the Molveno main body (von Wartburg et al., 2020), spans approximately ~6.8 to ~4.3 ka (Figs. 1, 12) and overlaps, within uncertainties, with the principal Middle Holocene age population identified at Lorei (5.21 ± 0.16 ka) and with the Middle Holocene chronological constraints obtained from Bergia-Sassere, Selvata, and Costa Lucanica. The younger group comprises events between ~1.4 and ~0.6 ka (Figs. 1, 12), Varini (Orombelli and Sauro, 1988), Castelpietra (Ivy-Ochs et al., 2017b), Kas (Ivy-Ochs et al., 2017a), and the Pra del Lago rockslide (Castellarin et al., 2005), which overlap with the Glare deposits in the northern Tovel Valley (Fig. 12). The Lavini di Marco rock avalanche at 3.0 ± 0.4 ka (Martin et al., 2014), together with the smaller Nembia event at Molveno (von Wartburg et al., 2020), stands out as a notable exception within this simple two-cluster framing (Fig. 12).

An additional regional archive comes from Lake Ledro mass-flow deposits interpreted as earthquake-related (Simonneau et al., 2013): twelve events were recorded over the last eight millennia, five of which occur within the same broad time intervals as the two landslide groups (Fig. 12). While such correspondences do not establish causation, they reinforce the observation that multiple slope-failure and sediment-remobilization records recur within similar Holocene times in this region.

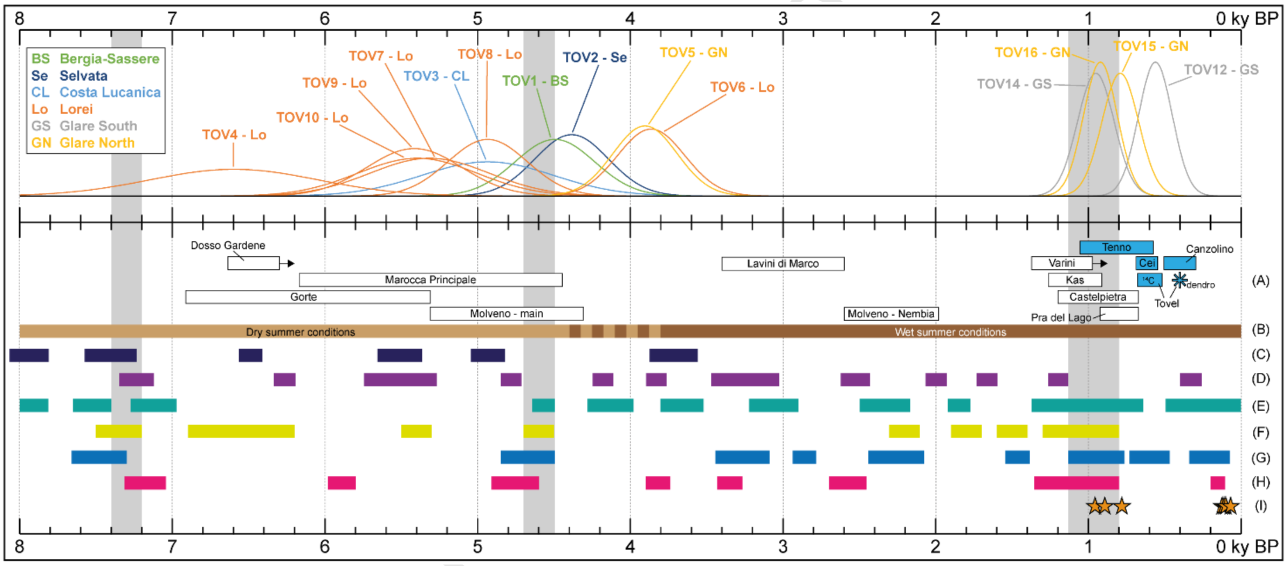

Figure 12: timeline highlighting key events and trends in the Tovel Valley and surrounding region. ^{36}Cl ages from this study are color-coded by deposit. (A) Dated landslides near the study area in white (Viganò et al., 2021) and dated submerged forests in the Trentino lakes in blue (Alessio et al., 1973, 1975, 1978; Biondi et al., 1981; Barbina et al., 1984). (B) Mediterranean-scale summer hydroclimatic phases inferred from lake-level records, showing alternations of wetter and drier summer conditions (Magny et al., 2013). (C) Warm and wet winter periods recorded in Ernesto Cave speleothems (Scholz et al., 2012). (D) Highstand levels at Lake Ledro (Magny et al., 2012). (E) flood-related deposits at Lake Ledro (Vannière et al., 2013). (F) Frequent flooding periods in the Venetian-Friulian alluvial plain (Rossato et al., 2015). (G) Frequent flooding periods in European alluvial plains (Benito et al., 2015). (H) Earthquake-related deposits at Lake Ledro (Simonneau et al., 2013). (I) Historical earthquakes in the study area with reconstructed Me ≥ 5, including the strong AD 1046, AD 1117 and AD 1222 events (Fig. 1; Guidoboni et al., 2018, 2019).

The regional significance of valley damming is also supported by the occurrence of submerged forests in landslide-dammed lakes in Trentino. Radiocarbon-dated drowned forests at Canzolino (1440-1642 AD; Alessio et al., 1975; Biondi et al., 1981), Cei (1271-1397 AD; Alessio et al., 1975; Biondi et al., 1981), and Tenno (893-1377 AD; Alessio et al., 1973, 1975, 1978; Biondi et al., 1981) overlap broadly with the younger landslide cluster at Tovel. The submerged forest of Lake Tovel yielded a radiocarbon age of 1283-1421 AD (Barbina et al., 1984). This is older than the dendrochronological evidence indicating drowning in 1597-1598 (Oetheimer, 1989), but overlaps with radiocarbon ages obtained from other drowned forests in the region. This discrepancy can be reconciled by the old-wood effect (Schiffer, 1986; Wood et al., 2024), particularly because the Tovel sample was taken from inner parts of an uprooted large tree (Biondi et al., 1981; Barbina et al., 1984).

5.3 Landslides in carbonate: main drivers in the Trentino area

The landslide events discussed above share long-term predisposing conditions linked to the carbonate successions of the southern Alps. Carbonate rocks are highly susceptible to dissolution, promoting extensive cracking and the development of karst networks (Borsato, 2007). Karst development has been active since at least the Miocene (Sauro et al., 2021) and currently sustains large aquifers (Dal Piaz et al., 2007); in the Tovel Valley, karst springs contribute to Lake Tovel and influence water-level variability (Ferretti and Borsato, 2006b; Bertagnoli et al., 2006). Such networks weaken rock masses, reducing stability and predisposing slopes to large failures (Pánek et al., 2009; Santo et al., 2007; Parise, 2008; Feng et al., 2014; Andriani and Parise, 2017).

Glacial and paraglacial inheritance provides a second major preconditioning framework. During the LGM, the Tovel Valley was occupied by a thick glacier tributary of the Adige-Sarca ice network (Monegato et al., 2017), and LGM ice filled the valleys where many dated landslides are found (Viganò et al., 2021). Glacial erosion produced U-shaped cross-sections and steepened valley walls; glaciokarst and associated stress redistribution may have promoted crack initiation and propagation, thereby enhancing the susceptibility of carbonate slopes to later Holocene failures.

Climatic variability can further contribute to progressive rock-mass degradation through hydromechanical stress during periods of intense rainfall (Preisig et al., 2015). Regional to continental reconstructions document phases of increased flooding and hydrological instability relevant to the study area (Lake Ledro: Vannière et al., 2013; Magny et al., 2012; Friulian-Venetian plain: Rossato et al., 2015; Europe-wide: Benito et al., 2015), supported by broader Mediterranean multiproxy records (Magny et al., 2013) and by stalagmite evidence from Ernesto Cave (~60 km SE of Tovel; Scholz et al., 2012). Periods of widespread climate deterioration with frequent summer precipitation and floods are known around ~7.4, ~4.6, ~2.3, and ~1.1 ka (Fig. 12; Vannière et al., 2013; Benito et al., 2015; Rossato et al., 2015; Mozzi et al., 2020). The climatic conditions occurring during these events are likely to promote the destabilization of already weakened rock masses. Given the large time-frames involved, these events cannot uniquely identify the short-term trigger of individual failures.

A third set of long-term drivers relates to regional tectonic architecture. The Southern Alps host major fault networks linked primarily to the NNE-SSW Giudicarie and NW-SE Schio-Vicenza systems (Castellarin et al., 2006; Viganò et al., 2018), including the Flavona-Val Strangola system cutting the Brenta Dolomites (Fig. 3). Interaction of these lineaments created anisotropies from metre to kilometre scale, lowering internal strength (Stead and Wolter, 2015). In this context, repeated deformation and long-term seismic shaking may contribute to the progressive weakening of rock masses (Rossato et al., 2020; Viganò and Scafidi, 2020; Wolter et al., 2020 and references therein).

Additional evidence of late Quaternary and Holocene tectonic activity is available in the Garda-Baldo-Lessini sector and adjacent Po Plain. Paleoseismological trenching at the Naole and Orsara fault scarps documented repeated Late Quaternary surface deformation, although chronological constraints remain broad and some structures may include a gravitational component (Galadini et al., 2001; Sauro and Zampieri, 2001). In the Brescia piedmont belt, active fault-related folding, surface faulting and liquefaction features associated with the Capriano del Colle fault system indicate persistent tectonic activity and strong local earthquakes during the late Quaternary (Livio et al., 2009). Regional syntheses further identify several potentially seismogenic structures in the Lake Garda area and discuss their possible role in generating major historical earthquakes (Berlusconi et al., 2013; Scardia et al., 2015).

The Tovel Valley lies near the junction of several tectonic lineaments (Fig. 1; Viganò et al., 2015), and even if large earthquakes (Me ≥ 6.0) are rare in the historical records (Fig. 1; Guidoboni et al., 2018, 2019), moderate events could progressively fatigue fractured carbonate rock and contribute to long-term instability

(Viganò et al., 2015), as recognized in comparable settings (Friedmann et al., 2003; Stead and Eberhardt, 2013; Preisig et al., 2015; Gischig et al., 2016; Wolter et al., 2016; Singeisen et al., 2020).

More generally, landslide clustering in mountain belts is commonly associated with landscape adjustments (e.g., deglaciation-related debuttressing; Hilger et al., 2018; Carling et al., 2023), hydrological/climatic variability (Soldati et al., 2004; Zerathe et al., 2014), and seismic activity (Moreiras et al., 2015; Köpfli et al., 2017). Such drivers can act over broad areas but may produce asymmetric valley responses where predisposing factors are unevenly distributed (Hermanns et al., 2006; Crosta et al., 2017; Hilger et al., 2018). In the Tovel Valley, however, failures occurred on both valley flanks (Fig. 6), pointing to pervasive litho-structural susceptibility rather than a single-sided preconditioning control.

5.4 Possible triggers of the Tovel landslides

Within the long-term preconditioning framework described above, the occurrence of multiple large failures within broadly similar Holocene time brackets in Trentino, including those at Tovel, raises the possibility that some events were promoted by shared short-term triggers or by periods of enhanced triggering efficiency (Fig. 12). Such temporal groupings do not, however, demonstrate that the landslides shared a common trigger. Identifying the triggers of prehistoric landslides remains challenging, particularly when exposure ages overlap in uncertainty and when independent event markers are scarce. Large rock-slope failures may be triggered by pore-pressure changes, as proposed for the Vajont rock avalanche (Wolter et al., 2016), or by seismic shaking, as documented after the 2008 Wenchuan earthquake (Yin et al., 2009); in other cases, no external trigger can be identified as for the Randa events, in Switzerland (Loew et al., 2012; Stead and Eberhardt, 2013). Regionally comparable age groupings should therefore be interpreted primarily as evidence for periods of enhanced slope susceptibility, rather than as direct evidence of a single triggering mechanism.

Climatic variability may have influenced this susceptibility by progressively modifying rock-mass strength, fracture hydrology and, where present, ground ice within rock discontinuities. In particular, warming and degradation of permafrost can reduce the strength of ice-bearing discontinuities and promote progressive destabilisation of high-mountain rock slopes (Deline et al., 2021; Mamot et al., 2021) like is occurring today in the Alps (Ravanel and Deline, 2015; Weber et al., 2025). Such processes provide a possible climatic preconditioning mechanism for the older Tovel cluster, especially if permafrost could have occurred in the relevant source areas during the Middle Holocene. Warming should be regarded as a possible contributor to progressive rock-mass weakening, rather than as an identified short-term trigger of individual failures. Conversely, the main phase of the Little Ice Age (LIA, CE 1575-1860; Le Roy et al., 2024 and references therein) is not associated with documented large landslides in Trentino. Although the completeness of the regional inventory and the response of individual slopes must be considered, this absence provides no clear evidence that sustained climatic cooling alone promoted widespread large-slope failure. More generally, cooling may have favoured frost-related weathering, but persistent freezing of ice-bearing discontinuities may also have temporarily increased rock-mass strength. The LIA comparison therefore suggests that climate warming alone cannot be assumed to have acted as an immediate trigger.

Extreme precipitation and associated pore-pressure increases represent another possible trigger for large landslides (Crosta et al., 2004; Guzzetti et al., 2008; Loew et al., 2017). However, the available regional and local evidence does not reveal a systematic correspondence between the Tovel landslide clusters and the hydrological or flood-related events shown in Fig. 12. The response to the Vaia Storm provides a modern, although necessarily limited, comparison. This extreme event caused only minor landslides in the south-eastern Alps (Antonetti et al., 2022; Pellegrini et al., 2021), while generating abundant debris flows in the Gares Valley (Macchi et al., 2023), which has a geological and geomorphological setting comparable to Tovel. The scarcity of debris-flow evidence in the Tovel Valley likewise provides little positive support for recurrent extreme rainfall as the common or dominant trigger of the large blocky failures (Guzzetti et al., 2008).

Seismic triggering provides a plausible alternative short-term mechanism. As discussed in chapters 2.1 and 5.3, the study area is seismically active, although strong earthquakes are rare (Viganò et al., 2015; Guidoboni et al., 2018, 2019; Niederstätter et al., 2025). Minor shaking and/or prolonged seismic sequences can affect broad areas and may trigger landslides, especially where rock masses are already weakened and where other preparatory factors are present (Papadopoulos and Plessa, 2000; Delgado et al., 2011). In this context, it is noteworthy that the younger Tovel cluster broadly overlaps in time with the “Media valle dell’Adige” (1046 AD), “Veronese” (1117 AD), and “Basso bresciano” (1222 AD) earthquakes (Fig. 12), the strongest historical events documented in the region during the last two millennia. This chronological correspondence makes seismic triggering a plausible interpretation for at least some of the younger failures, but it does not identify which, if any, of these earthquakes triggered a particular landslide.

Some dated deposits (including Glare) lie far from reconstructed epicentres (Fig. 1), but remain within published maximum distances for disrupted landslides triggered by earthquakes (90 km for Mw = 6 and 200 km for Mw = 6.8; Keefer, 1984; Delgado et al., 2011). Moreover, seismic energy may be transmitted efficiently along fault systems, allowing triggering at comparatively long distances (Gorum et al., 2023). Additional support for regionally distributed seismic activity during the same period comes from independent records, including earthquake-triggered landslides and cave collapses in the Adige Valley (Frisia et al., 2005; Ivy-Ochs et al., 2017), as well as lacustrine sedimentary records from nearby alpine basins (Simonneau et al., 2013; Gasperini et al., 2020). Although these datasets do not identify a specific causative earthquake for the Tovel landslides, they indicate that strong seismic activity affected a broader sector of the Southern Alps during the time interval represented by the younger cluster. Seismic triggering also cannot be excluded for the older cluster. Middle Holocene sedimentary records from nearby alpine basins contain mass-wasting deposits interpreted as earthquake-induced, including those reported from Lake Ledro (Simonneau et al., 2013). In contrast to the younger cluster, however, the older Tovel landslides cannot be compared with historically documented earthquakes, and the available palaeoseismic records have broad chronological uncertainties and uncertain source attribution, indicating only that seismic disturbances occurred during a broadly compatible interval. It does not permit identification of a specific earthquake as the trigger of any individual Tovel failure.

Overall, the available evidence is consistent with climatic and environmental changes acting mainly as long-term preparatory factors by progressively reducing slope stability. Seismic shaking represents a plausible short-term trigger, particularly for the younger cluster, for which independent historical and palaeoseismic evidence is comparatively stronger. For the older cluster, both progressive climate-related weakening and seismic triggering remain possible, but neither can be linked conclusively to individual failures. A similar interpretation has been proposed for clustered landslides in the north-western sector of the Eastern Alps (Aksay et al., 2021; Oswald et al., 2021). The chronological overlap among Tovel landslide ages, climatic phases and records of seismic disturbance should therefore be regarded as evidence of compatibility, not of direct causation.

6. Conclusions

Integrated geomorphological mapping, high-resolution topographic analysis, and new ^{36}Cl exposure ages indicate that the large blocky deposits of the Tovel Valley are Holocene in age and represent multiple slope-failure events rather than a single Lateglacial episode. Exposure ages indicate Holocene emplacement and suggest two broad periods of landslide activity. An older Middle Holocene phase is represented by the principal Lorei age population (5.21 ± 0.16 ka) together with overlapping chronological constraints from Bergia-Sassere, Costa Lucanica, and Selvata, whereas younger exposure ages fall between ~1.0 and ~0.6 ka. These findings support a revision of long-standing interpretations that attributed the valley-filling blocky deposits to deglaciation and instead support a predominantly Middle-to-Late Holocene.

The integration of exposure ages with superposition relationships, deposit morphology, lithological assemblages, and inferred source areas allows reconstruction of a relative landslide sequence across the valley. Individual deposits are morphologically distinct and were sourced from both valley flanks, indicating repeated, independent failures under broadly similar predisposing conditions. Where exposure ages overlap, geomorphic relationships provide essential constraints on relative timing, highlighting the value of combining cosmogenic dating with detailed field-based geomorphic analysis in complex Alpine settings.

The spatial distribution and volumes of the dated deposits show that several failures were capable of partially or fully damming the valley, with direct implications for the evolution of Lake Tovel. The data are consistent with a multi-phase history of recurrent damming, partial breaching, and drainage re-organization, rather than a single long-lived lake episode. The Holocene age of the Lorei deposit, together with sedimentological and geomorphic evidence from the lake basin, supports the existence of earlier lacustrine or palustrine phases prior to the historically documented lake-level rise at the end of the sixteenth century.

The landslide sequence reflects the interplay of persistent, long-term predisposing factors, including thick carbonate successions affected by karst dissolution, inherited structural anisotropies, and glacial and paraglacial modification of valley geometry. Over millennial timescales, long-term climatic variability and short periods of intense precipitation are likely to contribute to progressive weakening of rock masses. Nonetheless, given the large uncertainties, these events cannot be invoked as unique explanations for the timing of individual failures. Within this framework, the temporal clustering of events suggests that short-term triggers operated during periods of heightened susceptibility.

Among the potential triggers, seismic shaking emerges as the most plausible regional triggering mechanism for the younger cluster, given its temporal correspondence with the strongest historically documented earthquakes and other independent records of regional seismic activity, and the known ability of moderate-to-strong seismic events to initiate landslides at considerable distances in preconditioned terrain. For the older cluster, trigger attribution remains more uncertain, but similar triggering mechanisms can be hypothesized. Overall, the Tovel Valley provides an illustrative example of repeated Holocene large landslides in an Alpine carbonate setting, emphasizing the importance of structural inheritance, karst processes, and episodic triggering in shaping long-term valley evolution and associated geomorphic hazards.

CRediT authorship contribution statement

Sandro Rossato: data curation; investigation; methodology; visualization; writing - original draft. **Silvana Martin:** conceptualization; funding acquisition; methodology; supervision; visualization; writing - original draft. **Susan Ivy-Ochs: c**onceptualization; data curation; funding acquisition; methodology; writing - review & editing. **Alfio Viganò:** conceptualization; investigation; methodology; writing - review & editing. **Giovanni Monegato:** investigation; visualization; writing - original draft. **Giacomo Prosser:** investigation; writing - review & editing. **Christof Vockenhuber:** data curation; investigation; methodology. **Manuel Rigo:** investigation; methodology; visualization; writing - review & editing.

Funding

This research was funded by the Department of Geosciences of the University of Padova, grant number "SID 2020"; project title: "Historic and prehistoric landslides in the Alps. Implications for new hazard maps in mountainous areas. Focus on the Lake Garda–Brenta Dolomites sector (NE Italy)".

Declaration of competing interest

The authors declare that they have no known competing financial interests or personal relationships that could have appeared to influence the work reported in this paper.

Acknowledgements

The authors are grateful to Paolo Campedel for the useful discussions and the help in the field surveys. The authors thanks also Matteo Visintainer for providing the panorama photo used in Figure 4 and Tiziano Camagna for the Lake Tovel sketches used in Figure 11.

Declaration of generative AI and AI-assisted technologies in the manuscript preparation process

During the preparation of this work the authors used Microsoft Copilot in order to revise the text for readability and grammar checking. After using this tool, the authors reviewed and edited the content as needed and take full responsibility for the content of the publication.

References

Aaron, J., McDougall, S., 2019. Rock avalanche mobility: The role of path material. Engineering Geology 257, 105126. https://doi.org/10.1016/j.enggeo.2019.05.003

Abele, G., 1994. Large Rockslides: Their Causes and Movement on Internal Sliding Planes. Mountain Research and Development 14, 315. https://doi.org/10.2307/3673727

Abele, G., 1997. Influence of glacier and climatic variation on rockslide activity in the Alps. In: Matthews J.A., Brunsden, B., Frenzel, B., Gläser, B., Weiss, M.M. (Eds.), Rapid Mass Movement as a Source of Climatic Evidence for the Holocene, Palaoklimaforschung, vol. 19. Fischer, Stuttgart, 1-6.

Abele, G.: Bergstürze in den Alpen. Ihre Verbreitung, Morphologie und Folgeerscheinungen, Wiss. Alpenvereinshefte 25, Deutscher Alpenverein, Munich, 1974.

Aghib, F.S., Muttoni, G., Norini, G., Mariani, G.S., Zerboni, A., De Franco, R., Di Capua, A., Tira, M.A., Brusamolino, A., Menici, S., Caielli, G., Groppelli, G., Piccin, A., 2024. The Pleistocene tectono-stratigraphic evolution of the northern Po Plain (Italy) around the Castenedolo and Ciliverghe hillocks. Quat. res. 117, 170–182. https://doi.org/10.1017/qua.2023.47

Aksay, S., Ivy-Ochs, S., Hippe, K., Grämiger, L., Vockenhuber, C., 2021. Slope Failure in a Period of Increased Landslide Activity: Sennwald Rock Avalanche, Switzerland. Geosciences 11, 331. https://doi.org/10.3390/geosciences11080331

Aldighieri, B., Testa, B., Bertini, A., 2016. 3D Exploration of the San Lucano Valley: Virtual Geo-routes for Everyone Who Would Like to Understand the Landscape of the Dolomites. Geoheritage 8, 77–90. https://doi.org/10.1007/s12371-015-0164-x

Alessio, M., Allegri, L., Bella, F., Improta, S., Belluomini, G., Calderoni, C., Cortesi, C., Manfra, L., Petrone, V., Fruscalzo, A., 1978. University of Rome Carbon-14 Dates XV. Radiocarbon 20, 68–78. https://doi.org/10.1017/S003382220000391X

Alessio, M., Bella, F., Improta, S., Belluomini, G., Calderoni, G., Cortesi, C., Manelli, G.L., Vigilante, A., 1975. University of Rome Carbon-14 Dates XIII. Radiocarbon 17, 313–327. https://doi.org/10.1017/S003382220005983X

Alessio, M., Bella, F., Improta, S., Belluomini, G., Cortesi, C., Manelli, G.L., 1973. University of Rome Carbon-14 Dates XI. Radiocarbon 15, 382–387. https://doi.org/10.1017/S0033822200001284

Alfimov, V., Ivy-Ochs, S., 2009. How well do we understand production of 36Cl in limestone and dolomite? Quaternary Geochronology 4, 462–474. https://doi.org/10.1016/j.quageo.2009.08.005

Andriani, G.F., Parise, M., 2017. Applying rock mass classifications to carbonate rocks for engineering purposes with a new approach using the rock engineering system. Journal of Rock Mechanics and Geotechnical Engineering 9, 364–369. https://doi.org/10.1016/j.jrmge.2016.12.001

Antonetti, G., Gentilucci, M., Aringoli, D., Pambianchi, G., 2022. Analysis of landslide Susceptibility and Tree Felling Due to an Extreme Event at Mid-Latitudes: Case Study of Storm Vaia, Italy. Land 11, 1808. https://doi.org/10.3390/land11101808

Audra, P., Bini, A., Gabrovšek, F., Häuselmann, P., Hobléa, F., Jeannin, P.-Y., Kunaver, J., Monbaron, M., Šušteršič, F., Tognini, P., Trimmel, H., Wildberger, A., 2006. Cave genesis in the Alps between the Miocene and today: a review. Zeitschrift für Geomorphologie 50, 153–176. https://doi.org/10.1127/zfg/50/2006/153

Baldi, E., 1941. Ricerche idrobiologiche sul lago di Tovel. Memorie del Museo di Storia Naturale della Venezia Tridentina 6, 1-297, 1941.

Barbina, V., Calligaris, F., Del Fabbro, A., Turello, A., 1984. Udine radiocarbon laboratory date list II. Radiocarbon 26 (2), 293-296.

Benito, G., Macklin, M.G., Panin, A., Rossato, S., Fontana, A., Jones, A.F., Machado, M. J., Matlakhova, E., Mozzi, P., Zielhofer, C.: Recurring flood distribution patterns related to short-term Holocene climatic variability, Sci. Rep.-UK, 5, 16398, https://doi.org/10.1038/srep16398, 2015.

Berlusconi, A., Ferrario, M.F., Livio, F., Michetti, A.M., Violante, C., Esposito, E., Porfido, S., Fiaccavento, P., Ripamonti, L., Roncoroni, M., 2013. Quaternary Faults and Seismic Hazard in the Lake Garda Area. Ingegneria Sismica, 30(1–2), 10–35.

Bertagnoli, A., Majone, B., Bellin, A., 2006. Il bilancio idrologico del Lago di Tovel. Studi Trentini di Scienze Naturali - Acta Biologica 81 (2), 225-239.

Biondi, E., Pedrotti, F., Tommasi, G., 1981. Relitti di antiche foreste sul fondo di alcuni laghi del Trentino. Studi Trentini di Scienze Naturali - Acta Biologica 58, 93-117.

Borsato, A., Ferretti, P., 2004. Monitoraggio idrometrico del Lago di Tovel e del suo bacino. Studi Trentini di Scienze Naturali - Acta Biologica 81 (2), 205-223.

Borsato, A., Frisia, S., Corradini, F., Longinelli, A., Artioli, G., Casagrande, S., Dell'Eva, I., Santuliana, E., Gialanella, S., Selmo, E., Angeli, P., Lutterotti, L., Lauro, C., Avanzini, M., 2000. Acquiferi carsici in Trentino: caratteristiche chimico-fisiche, vulnerabilità e inquinamento. Rapporto Interno Provincia Autonoma di Trento, 270 pp..

Borsato, A., 2001. Characterisation of a high-altitude alpine karst aquifer by means of temperature, conductivity and discharge monitoring (Centonia spring, Brenta Dolomites, N-Italy). In: Mudry, J., Zwahlen, F. (eds), Proceedings of 7th Conference on Limestone Hydrology and Fissured Media, 51-54.

Borsato, A., 2007. Gli acquiferi carsici delle Dolomiti di Brenta: risorse idriche e funzionamento idrogeologico. Memorie Istituto Italiano di Speleologia II, 49-56.

Camagna, T., Bezzi, A., Bezzi, L., Oetheimer, C., Forti, A., Bernabei, M., Uccelli, T., 2021. La foresta sommersa del "LagoRosso" - un decennio di ricerche sugli alberi presenti sul fondo del lago di Tovel. Natura Alpina 3-4, 47-76.

Caporali, A., Braitenberg, C., Massironi, M., 2005. Geodetic and hydrological aspects of the Merano earthquake of 17 July 2001. Journal of Geodynamics 39, 317–336. https://doi.org/10.1016/j.jog.2005.01.001

Carling, P.A., Jansen, J.D., Su, T., Andersen, J.L., Knudsen, M.F., 2023. Ice-buttressing-controlled rock slope failure on a cirque headwall, Lake District, UK. Earth Surf. Dynam. 11, 817–833. https://doi.org/10.5194/esurf-11-817-2023

Castellarin, A., Picotti, V., Cantelli, L., Claps, M., Trombetta, G., Selli, L., Carton, A., Borsato, A., Daminato, F., Nardin, M., Santuliana, E., Veronese, L., Bollettinari, G., 2005. Note Illustrative della Carta geologica d'Italia alla scala 1:50.000, F. 080 Riva del Garda, Servizio Geologico d'Italia - ISPRA. https://doi.org/10.15161/OAR.IT/211611

Castellarin, A., Vai, G.B., Cantelli, L., 2006. The Alpine evolution of the Southern Alps around the Giudicarie faults: A Late Cretaceous to Early Eocene transfer zone. Tectonophysics 414, 203–223. https://doi.org/10.1016/j.tecto.2005.10.019

Castellarin, A., 1972. Evoluzione paleotettonica sinsedimentaria del limite tra "Piattaforma Veneta" e "Bacino lombardo" a nord di Riva del Garda. Giornale di Geologia 38, 11-212.

Chardon, M., 1975. Les Préalpes lombardes et leurs bordures. Thesis, 654 pp..

Christl, M., Vockenhuber, C., Kubik, P.W., Wacker, L., Lachner, J., Alfimov, V., Synal, H.-A., 2013. The ETH Zurich AMS facilities: Performance parameters and reference materials. Nuclear Instruments and Methods in Physics Research Section B: Beam Interactions with Materials and Atoms 294, 29–38. https://doi.org/10.1016/j.nimb.2012.03.004

Clark, P.U., Dyke, A.S., Shakun, J.D., Carlson, A.E., Clark, J., Wohlfarth, B., Mitrovica, J.X., Hostetler, S.W., McCabe, A.M., 2009. The Last Glacial Maximum. Science 325, 710–714. https://doi.org/10.1126/science.1172873

Crosta, G.B., Chen, H., Lee, C.F., 2004. Replay of the 1987 Val Pola Landslide, Italian Alps. Geomorphology 60, 127–146. https://doi.org/10.1016/j.geomorph.2003.07.015

Crosta, G.B., Hermanns, R.L., Dehls, J., Lari, S., Sepulveda, S., 2017. Rock avalanches clusters along the northern Chile coastal scarp. Geomorphology 289, 27–43. https://doi.org/10.1016/j.geomorph.2016.11.024

Dal Piaz, G.V., Castellarin, A., Martin, S., Selli, L., Carton, A., Pellegrini, G.B., Casolari, E., Daminato, F., Montresor, L., Picotti, V., Prosser, G., Santuliana, E., Cantelli, L., 2007. Note Illustrative della Carta geologica d'Italia alla scala 1:50.000, F. 042 Malé, Servizio Geologico d'Italia - ISPRA. https://doi.org/10.15161/OAR.IT/211591

Damian, J., 1892. Seestudien I. - Seen in der Umgebung von Trient, Westlich der Etsch. Mitt. K.k. Geogr. Gesell. 35 (9-10), 471-539.

de Mortillet, G., 1861. Carte des anciens glaciers du versant méridional des Alpes. Atti Soc. Sc. Nat. 3: 459-466.

Delgado, J., Garrido, J., López-Casado, C., Martino, S., Peláez, J.A., 2011. On far field occurrence of seismically induced landslides. Engineering Geology 123, 204–213. https://doi.org/10.1016/j.enggeo.2011.08.002

Deline, P., Gruber, S., Amann, F., Bodin, X., Delaloye, R., Failletaz, J., Fischer, L., Geertsema, M., Giardino, M., Hasler, A., Kirkbride, M., Krautblatter, M., Magnin, F., McColl, S., Ravanel, L., Schoeneich, P., Weber, S., 2021. Ice loss from glaciers and permafrost and related slope instability in high-mountain regions, in: Snow and Ice-Related Hazards, Risks, and Disasters. Elsevier, pp. 501–540. https://doi.org/10.1016/B978-0-12-817129-5.00015-9

Doglioni, C., Bosellini, A., 1987. Eoalpine and mesoalpine tectonics in the Southern Alps. Geol Rundsch 76, 735–754. https://doi.org/10.1007/BF01821061

Feng, Z., Li, B., Yin, Y.P., He, K., 2014. Rockslides on limestone cliffs with subhorizontal bedding in the southwestern calcareous area of China. Nat. Hazards Earth Syst. Sci. 14, 2627–2635. https://doi.org/10.5194/nhess-14-2627-2014

Ferretti, P., Borsato, A., 2006a. Geologia e geomorfologia della Valle e del Lago di Tovel. Studi Trentini di Scienze Naturali - Acta Biologica 81 (2), 173-187.

Ferretti, P., Borsato, A., 2006b. Studio idrogeologico della Valle e del Lago di Tovel. Studi Trentini di Scienze Naturali - Acta Biologica 81 (2), 189-203.

Freshfield, D.W., 1875. Italian Alps: Sketches in the Mountains of Ticino, Lombardy, the Trentino, and Venetia. Longmans, Green, and Co., London, 385 pp..

Friedmann, S.J., Kwon, G., Losert, W., 2003. Granular memory and its effect on the triggering and distribution of rock avalanche events. J. Geophys. Res. 108, 2002JB002174. https://doi.org/10.1029/2002JB002174

Frisia, S., Borsato, A., Spötl, C., Villa, I.M., Cucchi, F., 2005. Climate variability in the SE Alps of Italy over the past 17 000 years reconstructed from a stalagmite record. Boreas 34, 445–455. https://doi.org/10.1080/03009480500231336

Fuganti, A., Morteani, G., 1999. La storia del Lago di Tovel in base ai sedimenti della Baia Rossa (Trentino). Geologia Tecnica and Ambientale 3, 21-32.

Fuganti, A., 1969. Le sorgenti dell'Acqua Santa (Val di Non, Trento). Studi Trentini di Scienze Naturali - Acta Biologica 46, 432-444.

Galadini, F., Galli, P., 1999. Palaeoseismology related to the displaced Roman archaeological remains at Egna (Adige Valley, northern Italy). Tectonophysics 308, 171–191. https://doi.org/10.1016/S0040-1951(99)00080-3

Gischig, V., Preisig, G., Eberhardt, E., 2016. Numerical Investigation of Seismically Induced Rock Mass Fatigue as a Mechanism Contributing to the Progressive Failure of Deep-Seated Landslides. Rock Mech Rock Eng 49, 2457–2478. https://doi.org/10.1007/s00603-015-0821-z

Görüm, T., Tanyas, H., Karabacak, F., Yılmaz, A., Girgin, S., Allstadt, K.E., Süzen, M.L., Burgi, P., 2023. Preliminary documentation of coseismic ground failure triggered by the February 6, 2023 Türkiye earthquake sequence. Engineering Geology 327, 107315. https://doi.org/10.1016/j.enggeo.2023.107315

Guidoboni, E., Ferrari, G., Mariotti, D., Comastri, A., Tarabusi, G., Sgattoni, G., Valensise, G., 2018. CFTI5Med, Catalogo dei Forti Terremoti in Italia (461 a.C.-1997) e nell'area Mediterranea (760 a.C.-1500). https://doi.org/10.6092/INGV.IT-CFTI5

Guidoboni, E., Ferrari, G., Tarabusi, G., Sgattoni, G., Comastri, A., Mariotti, D., Ciuccarelli, C., Bianchi, M.G., Valensise, G., 2019. CFTI5Med, the new release of the catalogue of strong earthquakes in Italy and in the Mediterranean area. Sci Data 6, 80. https://doi.org/10.1038/s41597-019-0091-9

Guzzetti, F., Peruccacci, S., Rossi, M., Stark, C.P., 2008. The rainfall intensity–duration control of shallow landslides and debris flows: an update. Landslides 5, 3–17. https://doi.org/10.1007/s10346-007-0112-1

Heim, A., 1932. Bergsturz und Menschenleben, Vierteljahrschr. Naturf. Ges. Zürich, 20, Beer and Co., Zurich, Switzerland.

Hermanns, R.L., Blikra, L.H., Naumann, M., Nilsen, B., Panthi, K.K., Stromeyer, D., Longva, O., 2006. Examples of multiple rock-slope collapses from Köfels (Ötz valley, Austria) and western Norway. Engineering Geology 83, 94–108. https://doi.org/10.1016/j.enggeo.2005.06.026

Hilger, P., Hermanns, R.L., Gosse, J.C., Jacobs, B., Etzelmüller, B., Krautblatter, M., 2018. Multiple rock-slope failures from Mannen in Romsdal Valley, western Norway, revealed from Quaternary geological mapping and10 Be exposure dating. The Holocene 28, 1841–1854. https://doi.org/10.1177/0959683618798165

Ivy-Ochs, S., 2015. Glacier variations in the European Alps at the end of the last glaciation. CIG 41, 295–315. https://doi.org/10.18172/cig.2750

Ivy-Ochs, S., Martin, S., Campedel, P., Hippe, K., Vockenhuber, C., Carugati, G., Rigo, M., Pasqual, D., Viganò, A., 2017a. Geomorphology and Age of Large Rock Avalanches in Trentino (Italy): Castelpietra, in: Mikoš, M., Vilímek, V., Yin, Y., Sassa, K. (Eds.), Advancing Culture of Living with Landslides. Springer International Publishing, Cham, pp. 347–353. https://doi.org/10.1007/978-3-319-53483-1_41

Ivy-Ochs, S., Martin, S., Campedel, P., Hippe, K., Vockenhuber, C., Carugati, G., Rigo, M., Pasqual, D., Viganò, A., 2017b. Geomorphology and Age of Large Rock Avalanches in Trentino (Italy): Castelpietra, in: Mikoš, M., Vilímek, V., Yin, Y., Sassa, K. (Eds.), Advancing Culture of Living with Landslides. Springer International Publishing, Cham, pp. 347–353. https://doi.org/10.1007/978-3-319-53483-1_41

Ivy-Ochs, S., Poschinger, A. v., Synal, H.-A., Maisch, M., 2009. Surface exposure dating of the Flims landslide, Graubünden, Switzerland. Geomorphology 103, 104–112. https://doi.org/10.1016/j.geomorph.2007.10.024

Ivy-Ochs, S., Synal, H.-A., Roth, C., Schaller, M., 2004. Initial results from isotope dilution for Cl and 36Cl measurements at the PSI/ETH Zurich AMS facility. Nuclear Instruments and Methods in Physics Research Section B: Beam Interactions with Materials and Atoms 223–224, 623–627. https://doi.org/10.1016/j.nimb.2004.04.115

Köpfli, P., Grämiger, L.M., Moore, J.R., Vockenhuber, C., Ivy-Ochs, S., 2018. The Oeschinensee rock avalanche, Bernese Alps, Switzerland: a co-seismic failure 2300 years ago? Swiss J Geosci 111, 205–219. https://doi.org/10.1007/s00015-017-0293-0

Kulbe, T., Anselmetti, F., Cantonati, M., Sturm, M., 2005. Environmental History of Lago di Tovel, Trento, Italy, Revealed by Sediment Cores and 3.5 kHz Seismic Mapping. J Paleolimnol 34, 325–337. https://doi.org/10.1007/s10933-005-5022-4

Le Roy, M., Ivy-Ochs, S., Nicolussi, K., Monegato, G., Reitner, J.M., Colucci, R.R., Ribolini, A., Spagnolo, M., Stoffel, M., 2024. Holocene glacier variations in the Alps, in: European Glacial Landscapes. Elsevier, pp. 367–418. https://doi.org/10.1016/B978-0-323-99712-6.00018-0

Lepsius, R., 1878. Das westliche Süd-Tirol: geologisch dargestellt. Verlag von W. Hertz (Bessersche Buchhandlung). 375 pp., Berlin.

Livio, F.A., Berlusconi, A., Michetti, A.M., Sileo, G., Zerboni, A., Trombino, L., Cremaschi, M., Mueller, K., Vittori, E., Carcano, C., Rogledi, S., 2009. Active fault-related folding in the epicentral area of the December 25, 1222 (Io=IX MCS) Brescia earthquake (Northern Italy): Seismotectonic implications. Tectonophysics 476, 320–335. https://doi.org/10.1016/j.tecto.2009.03.019

Loew, S., Gischig, V., Willenberg, H., Alpiger, A., Moore, J.R., 2012. Randa: Kinematics and driving mechanisms of a large complex rockslide, in: Clague, J.J., Stead, D. (Eds.), Landslides. Cambridge University Press, pp. 297–309. https://doi.org/10.1017/CBO9780511740367.025

Loew, S., Gschwind, S., Gischig, V., Keller-Signer, A., Valenti, G., 2017. Monitoring and early warning of the 2012 Preonzo catastrophic rockslope failure. Landslides 14, 141–154. https://doi.org/10.1007/s10346-016-0701-y

Macchi, G., Monegato, G., Pasuto, A., Boretto, G., Crema, S., Marchi, L., Cavalli, M., 2023. Geomorphology of the Liera catchment (Dolomites, NE Italy): understanding landscape response to an extreme event. Journal of Maps 19, 2165979. https://doi.org/10.1080/17445647.2023.2165979

Magny, M., Combourieu-Nebout, N., De Beaulieu, J.L., Bout-Roumazeilles, V., Colombaroli, D., Desprat, S., Francke, A., Joannin, S., Ortu, E., Peyron, O., Revel, M., Sadori, L., Siani, G., Sicre, M.A., Samartin, S., Simonneau, A., Tinner, W., Vannière, B., Wagner, B., Zanchetta, G., Anselmetti, F., Brugiapaglia, E., Chapron, E., Debret, M., Desmet, M., Didier, J., Essallami, L., Galop, D., Gilli, A., Haas, J.N., Kallel, N., Millet, L., Stock, A., Turon, J.L., Wirth, S., 2013. North–south palaeohydrological contrasts in the central Mediterranean during the Holocene: tentative synthesis and working hypotheses. Clim. Past 9, 2043–2071. https://doi.org/10.5194/cp-9-2043-2013

Magny, M., Joannin, S., Galop, D., Vannière, B., Haas, J.N., Bassetti, M., Bellintani, P., Scandolari, R., Desmet, M., 2012. Holocene palaeohydrological changes in the northern Mediterranean borderlands as reflected by the lake-level record of lake ledro, northeastern Italy. Quat. res. 77, 382–396. https://doi.org/10.1016/j.yqres.2012.01.005

Mamot, P., Weber, S., Eppinger, S., Krautblatter, M., 2021. A temperature-dependent mechanical model to assess the stability of degrading permafrost rock slopes. Earth Surf. Dynam. 9, 1125–1151. https://doi.org/10.5194/esurf-9-1125-2021

Martin, S., Campedel, P., Ivy-Ochs, S., Viganò, A., Alfimov, V., Vockenhuber, C., Andreotti, E., Carugati, G., Pasqual, D., Rigo, M., 2014. Lavini di Marco (Trentino, Italy): 36Cl exposure dating of a polyphase rock avalanche. Quaternary Geochronology 19, 106–116. https://doi.org/10.1016/j.quageo.2013.08.003

Monegato, G., Scardia, G., Hajdas, I., Rizzini, F., Piccin, A., 2017. The Alpine LGM in the boreal ice-sheets game. Sci Rep 7, 2078. https://doi.org/10.1038/s41598-017-02148-7

Montandon, F., 1933. Chronologie des grands éboulements alpins du début de l'ère chrétienne à nos jours. Matériaux pour l'étude des calamités 32, 271-340.

Moreiras, S.M., Hermanns, R.L., Fauqué, L., 2015. Cosmogenic dating of rock avalanches constraining Quaternary stratigraphy and regional neotectonics in the Argentine Central Andes (32° S). Quaternary Science Reviews 112, 45–58. https://doi.org/10.1016/j.quascirev.2015.01.016

Mozzi, P., Piovan, S., Corrò, E., 2020. Long-term drivers and impacts of abrupt river changes in managed lowlands of the Adige River and northern Po delta (Northern Italy). Quaternary International 538, 80–93. https://doi.org/10.1016/j.quaint.2018.10.024

Nicod, J., 1976. Les Dolomites de la Brenta (Italie). Karst haut-alpine typique et le probleme des cuvettes glacio-karstiques. Zeitschrift für Geomorphologie 26, 35-57.

Niederstätter, M., Wils, K., Ramisch, A., Haas, J.N., Pomella, H., Szidat, S., Strasser, M., Moernaut, J., 2025. Strong earthquake in a low seismicity area of the European Southern Alps during Roman Times – A lacustrine paleoseismic evaluation. Quaternary Science Reviews 357, 109341. https://doi.org/10.1016/j.quascirev.2025.109341

Oetheimer, C., 1989. Etude geomorphologique des eboulements remainies de la Vallee de Tovel: contribution à la connaissance des marocche du Trentin (Italie). Studi Trentini di Scienze Naturali - Acta Geologica 65, 3-47.

Oetheimer, C., 1990. La foresta sommersa del Lago di Tovel (Trentino): reinterpretazione e datazione dendrocronologica. Studi Trentini di Scienze Naturali - Acta Geologica 67, 3-23.

Orombelli, G., Sauro, U., 1988. I Lavini Di Marco: Un Gruppo Di Frane Oloceniche Nel Contesto Morfoneotettonico Dell'alta Val Lagarina (Trentino). Supplementi di Geografia Fisica E Dinamica Quaternaria 1, 107-116, 1988.

Ostermann, M., Sanders, D., 2017. The Benner pass rock avalanche cluster suggests a close relation between long-term slope deformation (DSGSDs and translational rock slides) and catastrophic failure. Geomorphology 289, 44–59. https://doi.org/10.1016/j.geomorph.2016.12.018

Oswald, P., Moernaut, J., Fabbri, S.C., De Batist, M., Hajdas, I., Ortner, H., Titzler, S., Strasser, M., 2021. Combined On-Fault and Off-Fault Paleoseismic Evidence in the Postglacial Infill of the Inner-Alpine Lake Achensee (Austria, Eastern Alps). Front. Earth Sci. 9, 670952. https://doi.org/10.3389/feart.2021.670952

Pánek, T., Hradecký, J., Šilhán, K., Smolková, V., Altová, V., 2009. Time constraints for the evolution of a large slope collapse in karstified mountainous terrain of the southwestern Crimean Mountains, Ukraine. Geomorphology 108, 171–181. https://doi.org/10.1016/j.geomorph.2009.01.003

Papadopoulos, G.A., Plessa, A., 2000. Magnitude–distance relations for earthquake-induced landslides in Greece. Engineering Geology 58, 377–386. https://doi.org/10.1016/S0013-7952(00)00043-0

Parise, M., 2008. Rock failures in karst, in Chen, Z., Zhang, J.-M., Ho, K., Wu, F.-Q., Li, Z.-K. (Eds.), Landslides and Engineered Slopes. From the Past to the Future, CRC Press, pp. 297-302.

Pellegrini, G., Martini, L., Cavalli, M., Rainato, R., Cazorzi, A., Picco, L., 2021. The morphological response of the Tegnas alpine catchment (Northeast Italy) to a Large Infrequent Disturbance. Science of The Total Environment 770, 145209. https://doi.org/10.1016/j.scitotenv.2021.145209

Penck, A., Brückner, E., 1909. Die Alpen im Eiszeitalter. Bd. 3. Die Eiszeiten in den Südalpen in dem Bereich der Ostabdachung der Alpen. Tauchnitz, Leipzig, 482 pp..

Perna, G., Sauro, U., 1979. Aspects de la dénudation karstique des "marocche". Actes Symposium Internationale Erosion Karstique, 97-103.

Picotti, V., Casolari, E., Castellarin, A., 1998. Mesozoic basin evolution of the Central South-Alpine (Giudicarie): from Norian-Liassic rifting to the Mid-Late Cretaceous foreland transpression (partial basin inversion), in Martin, S., Godard, G., Ranalli, G. (Eds.), Evolution of the deep crust in the central and eastern Alps. Field excursion guide. Memorie di Scienze Geologiche 50, pp. 96-99.

Prager, C., Zangerl, C., Patzelt, G., Brandner, R., 2008. Age distribution of fossil landslides in the Tyrol (Austria) and its surrounding areas. Nat. Hazards Earth Syst. Sci. 8, 377–407. https://doi.org/10.5194/nhess-8-377-2008

Preisig, G., Gischig, V., Eberhardt, E., Hungr, O., 2015. Hydromechanical versus seismic fatigue in progressive failure of deepseated landslides, in: 13th ISRM International Congress of Rock Mechanics. International Society for Rock Mechanics and Rock Engineering, 10-13 May 2015, Montreal, Canada.

Prosser, G., 2000. The development of the North Giudicarie fault zone (Insubric line, Northern Italy). Journal of Geodynamics 30, 229–250. https://doi.org/10.1016/S0264-3707(99)00035-6

Prosser, G., 1998. Strike-slip movements and thrusting along a transpressive fault zone: The North Giudicarie line (Insubric line, northern Italy). Tectonics 17, 921–937. https://doi.org/10.1029/1998TC900010

Ravanel, L., Deline, P., 2015. Rockfall Hazard in the Mont Blanc Massif Increased by the Current Atmospheric Warming, in: Lollino, G., Manconi, A., Clague, J., Shan, W., Chiarle, M. (Eds.), Engineering Geology for Society and Territory - Volume 1. Springer International Publishing, Cham, pp. 425–428. https://doi.org/10.1007/978-3-319-09300-0_81

Ravazzi, C., Pini, R., Badino, F., De Amicis, M., Londeix, L., Reimer, P.J., 2014. The latest LGM culmination of the Garda Glacier (Italian Alps) and the onset of glacial termination. Age of glacial collapse and vegetation chronosequence. Quaternary Science Reviews 105, 26–47. https://doi.org/10.1016/j.quascirev.2014.09.014

Rettig, L., Rossato, S., Kamleitner, S., Mozzi, P., Ivy-Ochs, S., Marcato, E., Christl, M., Martin, S., Monegato, G., 2025. The Last Glacial Maximum (LGM) glacier network of the Valsugana area (south-eastern European Alps and Prealps, NE Italy). E&G Quaternary Sci. J. 74, 151–168. https://doi.org/10.5194/egqsj-74-151-2025

Rossato, S., Fontana, A., Mozzi, P., 2015. Meta-analysis of a Holocene 14C database for the detection of paleohydrological crisis in the Venetian–Friulian Plain (NE Italy). CATENA 130, 34–45. https://doi.org/10.1016/j.catena.2014.10.033

Rossato, S., Ivy-Ochs, S., Martin, S., Viganò, A., Vockenhuber, C., Rigo, M., Monegato, G., De Zorzi, M., Surian, N., Campedel, P., Mozzi, P., 2020. Timing, drivers and impacts of the historic Masiere di Vedana rock avalanche (Belluno Dolomites, NE Italy). Nat. Hazards Earth Syst. Sci. 20, 2157–2174. https://doi.org/10.5194/nhess-20-2157-2020

Rovida, A., Antonucci, A., Locati, M., 2022. The European Preinstrumental Earthquake Catalogue EPICA, the 1000–1899 catalogue for the European Seismic Hazard Model 2020. Earth Syst. Sci. Data 14, 5213–5231. https://doi.org/10.5194/essd-14-5213-2022

Rovida, A.N., Albini, P., Locati, M., Antonucci, A., 2020. Insights into Preinstrumental Earthquake Data and Catalogs in Europe. Seismological Research Letters 91, 2546–2553. https://doi.org/10.1785/0220200058

Ruggia, G., Ivy-Ochs, S., Aaron, J., Steinemann, O., Martin, S., Rigo, M., Rossato, S., Vockenhuber, C., Monegato, G., Viganò, A., 2021. Reconstructing the Gorte and Spiaz de Navesele Landslides, NE of Lake Garda, Trentino Dolomites (Italy). Geosciences 11, 404. https://doi.org/10.3390/geosciences11100404

Sacco, F., 1940. Le Marocche del Veneto. L'Universo 21 (11), 750-782.

Samia, J., Temme, A., Bregt, A., Wallinga, J., Guzzetti, F., Ardizzone, F., Rossi, M., 2017. Do landslides follow landslides? Insights in path dependency from a multi-temporal landslide inventory. Landslides 14, 547–558. https://doi.org/10.1007/s10346-016-0739-x

Santo, A., Del Prete, S., Di Crescenzo, G., Rotella, M., 2007. Karst processes and slope instability: some investigations in the carbonate Apennine of Campania (southern Italy). SP 279, 59–72. https://doi.org/10.1144/SP279.6

Sauro, F., Fellin, M.G., Columbu, A., Häuselmann, P., Borsato, A., Carbone, C., De Waele, J., 2021. Hints on the Late Miocene Evolution of the Tonale-Adamello-Brenta Region (Alps, Italy) Based on Allochtonous Sediments From Raponzolo Cave. Front. Earth Sci. 9, 672119. https://doi.org/10.3389/feart.2021.672119

Sauro, U., Zampieri, D., 2001. Evidence of recent surface faulting and surface rupture in the Fore-Alps of Veneto and Trentino (NE Italy). Geomorphology 40 (3-4), 169-184, https://doi.org/10.1016/S0169-555X(01)00041-1

Scardia, G., Festa, A., Monegato, G., Pini, R., Rogledi, S., Tremolada, F., Galadini, F., 2015. Evidence for late Alpine tectonics in the Lake Garda area (northern Italy) and seismogenic implications. Geological Society of America Bulletin 127, 113–130. https://doi.org/10.1130/B30990.1

Schiffer, M.B., 1986. Radiocarbon dating and the “old wood” problem: The case of the Hohokam chronology. Journal of Archaeological Science 13, 13–30. https://doi.org/10.1016/0305-4403(86)90024-5

Scholz, D., Frisia, S., Borsato, A., Spötl, C., Fohlmeister, J., Mudelsee, M., Miorandi, R., Mangini, A., 2012. Holocene climate variability in north-eastern Italy: potential influence of the NAO and solar activity recorded by speleothem data. Climate of the Past 8, 1367–1383. https://doi.org/10.5194/cp-8-1367-2012

Schwinner, R., 1912. Der Monte Spinale bei Campiglio und andere Bergstürze in den Südalpen. Mitteilungen der Geologischen Gesellschaft in Wien 5, 128-197.

Simonneau, A., Chapron, E., Vannière, B., Wirth, S.B., Gilli, A., Di Giovanni, C., Anselmetti, F.S., Desmet, M., Magny, M., 2013. Mass-movement and flood-induced deposits in Lake Ledro, southern Alps, Italy: implications for Holocene palaeohydrology and natural hazards. Clim. Past 9, 825–840. https://doi.org/10.5194/cp-9-825-2013

Singeisen, C., Ivy-Ochs, S., Wolter, A., Steinemann, O., Akçar, N., Yesilyurt, S., Vockenhuber, C., 2020. The Kandersteg rock avalanche (Switzerland): integrated analysis of a late Holocene catastrophic event. Landslides 17, 1297–1317. https://doi.org/10.1007/s10346-020-01365-y

Slejko, D., 1989. Sismica attuale nell'area benacense. In: Il rischio sismico nel Bresciano. Editoriale Ramperto, pp. 31-39.

Soldati, M., Corsini, A., Pasuto, A., 2004. Landslides and climate change in the Italian Dolomites since the Late glacial. CATENA 55, 141–161. https://doi.org/10.1016/S0341-8162(03)00113-9

Stead, D., Eberhardt, E., 2013. Understanding the mechanics of large landslides, Italian Journal of Engineering Geology and Environment - Book Series 6, 85-112, https://doi.org/10.4408/IJEGE.2013-06.B-07

Stead, D., Wolter, A., 2015. A critical review of rock slope failure mechanisms: The importance of structural geology. Journal of Structural Geology 74, 1–23. https://doi.org/10.1016/j.jsg.2015.02.002

Stone, J.O., 2000. Air pressure and cosmogenic isotope production. J. Geophys. Res. 105, 23753–23759. https://doi.org/10.1029/2000JB900181

Stoppani, A., 1878. Carattere marino dei grandi anfiteatri morenici dell'alta Italia. In: Vallardi, F. (Ed), Geologia d'Italia, 78 pp..

Styllas, M.N., Schimmelpfennig, I., Benedetti, L., Ghilardi, M., Aumaître, G., Bourlès, D., Keddadouche, K., 2018. Late-glacial and Holocene history of the northeast Mediterranean mountain glaciers - New insights from in situ-produced 36Cl-based cosmic ray exposure dating of paleo-glacier deposits on Mount Olympus, Greece. Quaternary Science Reviews 193, 244–265. https://doi.org/10.1016/j.quascirev.2018.06.020

Taramelli, T., 1881. Di alcuni scoscendimenti postglaciali sulle Alpi Meridionali. Rendiconti del Reale Istituto Lombardo di Scienze e Lettere 7 (14), 74-81.

Tarquini, S., Isola, I., Favalli, M., Battistini, A., Dotta, G., 2023. TINITALY, a digital elevation model of Italy with a 10 meters cell size, version 1.1. https://doi.org/10.13127/TINITALY/1.1

Tarquini, S., Isola, I., Favalli, M., Mazzarini, F., Bisson, M., Pareschi, M.T., Boschi, E., 2007. TINITALY/01: a new Triangular Irregular Network of Italy. Annals of Geophysics 50, 407–425. https://doi.org/10.4401/ag-4424

Trener, G.B., 1924. Geologia delle Marocche. In: Gli impianti idroelettrici della Città di Trento, Parte II, 25-33.

Trevisan, L., 1939. Il Gruppo di Brenta (Trentino occidentale), Memorie dell'Istituto Geologico della Reale Università di Padova 13, 128 pp..

Vannière, B., Magny, M., Joannin, S., Simonneau, A., Wirth, S.B., Hamann, Y., Chapron, E., Gilli, A., Desmet, M., Anselmetti, F.S., 2013. Orbital changes, variation in solar activity and increased anthropogenic activities: controls on the Holocene flood frequency in the Lake Ledro area, Northern Italy. Clim. Past 9, 1193–1209. https://doi.org/10.5194/cp-9-1193-2013

Venzo, G.A., 1960. Fenomeni franosi nel Trentino. Memorie del Museo di Storia Naturale della Venezia Tridentina 13(2), 79-82.

Viganò, A., Rossato, S., Martin, S., Ivy-Ochs, S., Zampieri, D., Rigo, M., Monegato, G., 2021. Large landslides in the Alpine valleys of the Giudicarie and Schio-Vicenza tectonic domains (NE Italy). Journal of Maps 17, 197–208. https://doi.org/10.1080/17445647.2021.1880979

Viganò, A., Scafidi, D., 2020. EARTHQUAKE LOCATIONS AND THEIR INTERPRETATION: BRIDGING THE GAP BETWEEN SEISMOLOGICAL DATA AND GEOLOGICAL PHENOMENA. Alpine and Mediterranean Quaternary 33, 149–156. https://doi.org/10.26382/AMQ.2020.06

Viganò, A., Scafidi, D., Ranalli, G., Martin, S., Della Vedova, B., Spallarossa, D., 2015. Earthquake relocations, crustal rheology, and active deformation in the central–eastern Alps (N Italy). Tectonophysics 661, 81–98. https://doi.org/10.1016/j.tecto.2015.08.017

Viganò, A., Zampieri, D., Rossato, S., Martin, S., Selli, L., Prosser, G., Ivy-Ochs, S., Campedel, P., Fedrizzi, F., Franceschi, M., Rigo, M., 2018. Past to present deformation of the central-eastern Southern Alps: from the foreland to the Giudicarie belt. GFT 10, 1–78. https://doi.org/10.3301/GFT.2018.01

Vockenhuber, C., Miltenberger, K.-U., Synal, H.-A., 2019. 36Cl measurements with a gas-filled magnet at 6 MV. Nuclear Instruments and Methods in Physics Research Section B: Beam Interactions with Materials and Atoms 455, 190–194. https://doi.org/10.1016/j.nimb.2018.12.046

von Wartburg, J., Ivy-Ochs, S., Aaron, J., Martin, S., Leith, K., Rigo, M., Vockenhuber, C., Campedel, P., Viganò, A., 2020. Constraining the Age and Source Area of the Molveno landslide Deposits in the Brenta Group, Trentino Dolomites (Italy). Front. Earth Sci. 8, 164. https://doi.org/10.3389/feart.2020.00164

Weber, S., Beutel, J., Dietze, M., Bast, A., Kenner, R., Phillips, M., Leinauer, J., Mühlbauer, S., Pfluger, F., Krautblatter, M., 2025. Progressive destabilization of a freestanding rock pillar in permafrost on the Matterhorn (Swiss Alps): Hydro-mechanical modeling and analysis. Earth Surf. Dynam. 13, 1157–1179. https://doi.org/10.5194/esurf-13-1157-2025

Wiebols, J., 1938. Geologie der Brentagruppe. Jahrbuch der Geologischen Bundesanstalt 88 (3-4), 261-350.

Wolter, A., 2020. A review of methods used to investigate structural control on slope instability. Alpine and Mediterranean Quaternary 33, 139–147. https://doi.org/10.26382/AMQ.2020.05

Wolter, A., Gischig, V., Stead, D., Clague, J.J., 2016. Investigation of Geomorphic and Seismic Effects on the 1959 Madison Canyon, Montana, Landslide Using an Integrated Field, Engineering Geomorphology Mapping, and Numerical Modelling Approach. Rock Mech Rock Eng 49, 2479–2501. https://doi.org/10.1007/s00603-015-0889-5

Wolter, A., Stead, D., Ward, B.C., Clague, J.J., Ghirotti, M., 2016. Engineering geomorphological characterisation of the Vajont Slide, Italy, and a new interpretation of the chronology and evolution of the landslide. Landslides 13, 1067–1081. https://doi.org/10.1007/s10346-015-0668-0

Wood, R., King, F., Esmay, R., Chen, Q., Schneider, L., Dotte-Sarout, E., Fallon, S., Fryirs, K., Gillespie, R., Blong, R., 2024. The size inherited age effect on radiocarbon dates of alluvial deposits: redating charcoal fragments in a sand-bed stream, MacDonald River, NSW, Australia. Radiocarbon 66, 1006–1019. https://doi.org/10.1017/RDC.2023.75

Yin, Y., Wang, F., Sun, P., 2009. Landslide hazards triggered by the 2008 Wenchuan earthquake, Sichuan, China. Landslides 6, 139–152. https://doi.org/10.1007/s10346-009-0148-5

Zerathe, S., Lebourg, T., Braucher, R., Bourlès, D., 2014. Mid-Holocene cluster of large-scale landslides revealed in the Southwestern Alps by 36Cl dating. Insight on an Alpine-scale landslide activity. Quaternary Science Reviews 90, 106–127. https://doi.org/10.1016/j.quascirev.2014.02.015

Highlights

- Six different deposits are dated to the Holocene and record multiple landslides
- ^{36}Cl exposure ages define two Holocene landslide clusters (6.6-3.9 and 1.0-0.6 ka)
- Lake Tovel repeatedly formed in a landslide-dammed depression during the Holocene
- Failures from both valley flanks repeatedly dammed and reorganized drainage
- Temporal clustering suggests episodic triggering on long-term preconditioned slopes